Nuclear Medicine and Biology 94–95 (2021) 53–66

Contents lists available at ScienceDirect

Nuclear Medicine and Biology

journal homepage: www.elsevier.com/locate/nucmedbio

Towards the development of a targeted albumin-binding radioligand: Synthesis, radiolabelling and preliminary *in vivo* studies

Cathryn Helena Stanford Driver [a], Thomas Ebenhan [a], Zoltan Szucs [c], Mohammed Iqbal Parker [d], Jan Rijn Zeevaart [a,e,*], Roger Hunter [b]

[a] South African Nuclear Energy Corporation, Radiochemistry and NuMeRI PreClinical Imaging Facility, Elias Motsoaledi Street, R104 Pelindaba, North West 0240, South Africa
[b] Department of Chemistry, University of Cape Town, Cape Town, South Africa
[c] MTA Atomki, Debrecen, Hungary
[d] Department of Medical Biochemistry and Institute for Infectious Disease and Molecular Medicine, University of Cape Town Medical School, University of Cape Town, Cape Town, South Africa
[e] Preclinical Drug Development Platform, North West University, Potchefstroom, South Africa

ARTICLE INFO

Article history:
Received 6 October 2020
Received in revised form 14 December 2020
Accepted 2 January 2021

Keywords:
Cancer
Radiopharmaceuticals
Macrocyclic ligands
Copper-64
Albumin-binding

ABSTRACT

Introduction: The compound named 4-[10-(4-(2,5-dioxo-2,5-dihydro-1H-pyrrol-1-yl)butanamido)decyl]-11-[10-(β,D-glucopyranos-1-yl)-1-oxodecyl]-1,4,8,11-tetraazacyclotetradecane-1,8-diacetic acid is a newly synthesised molecule capable of binding *in vivo* to albumin to form a bioconjugate. This compound was given the name, GluCAB(glucose-chelator-albumin-binder)-maleimide-**1**. Radiolabelled GluCAB-maleimide-**1** and subsequent bioconjugate is proposed for prospective oncological applications and works on the theoretical dual-targeting principle of tumour localization through the "enhanced permeability and retention (EPR) effect" and glucose metabolism.

Methods: The precursor, GluCAB-amine-**2**, and subsequent GluCAB-maleimide-**1** was synthesised *via* sequential regioselective, distal N-functionalisation of a cyclam template with a tether containing a synthetically-derived β-glucoside followed by a second linker to incorporate a maleimide moiety for albumin-binding. GluCAB-amine-**2** was radiolabelled with [^{64}Cu]$CuCl_2$ in 0.1 M NH_4OAc (pH 3.5, 90 °C, 30 min), purified and converted post-labeling in 0.01 M PBS to [^{64}Cu]Cu-GluCAB-maleimide-**1**. Serum stability and protein binding studies were completed according to described methods. Healthy BALB/c ice (three groups of $n = 5$) were injected intravenously with [^{64}Cu]Cu-TETA, [^{64}Cu]Cu-GluCAB-amine-**2** or [^{64}Cu]Cu-GluCAB-maleimide-**1** and imaged using microPET/CT at 1, 2, 4, 8 and 24 h post-injection. Biodistribution of the compounds were determined *ex vivo* after 24 h using gamma counting.

Results: GluCAB-maleimide-**1** was synthesised in five consecutive steps with an overall yield of 11%. [^{64}Cu]Cu-GluCAB-amine-**2** (97% labelling efficiency) was converted to [^{64}Cu]Cu-GluCAB-maleimide-**1** (93% conversion; 90% radiochemical purity). Biodistribution analysis indicated that the control compounds were rapidly and almost completely excreted as compared to [^{64}Cu]Cu-GluCAB-maleimide-**1** that exhibited a prolonged biological half-life (6–8 h). Both, [^{64}Cu]Cu-GluCAB-maleimide-**1** and -amine-**2** were excreted through the hepatobiliary system but a higher hepatic presence of the albumin-bound compound was noted.

Conclusions, advances in knowledge and implications for patient care: This initial evaluation paves the way for further investigation into the tumour targeting potential of [^{64}Cu]Cu-GluCAB-maleimide-**1**. An efficient targeted radioligand will allow for further development of a prospective theranostic agent for more personalized patient treatment which potentially improves overall patient prognosis, outcome and health care.

1. Introduction

The principle of targeted cancer diagnosis or treatment involves the use of drug-delivery systems that improve the efficiency of drug uptake by the tumour [1]. In designing a selective cancer targeting agent, it is necessary therefore to understand cancer-cell tumourigenesis and the tumour micro-environment. Tumours develop as a result of cancerous cells that are fast-growing and which over-express many cell-surface receptors, each associated with the provision of metabolites for cell growth and division [2]. New cancer diagnostics or therapeutics can be designed to have a high affinity for one of these up-regulated cancer cell-surface receptors leading to the compound's accumulation within the tumour cell ('Active' targeting). Active targeting ligands include monoclonal antibodies (mAbs) as well as antibody fragments, proteins,

* Corresponding author at: Preclinical Drug Development Platform, North West University, Potchefstroom, South Africa.
E-mail address: janrijn.zeevaart@necsa.co.za (J.R. Zeevaart).

https://doi.org/10.1016/j.nucmedbio.2021.01.001
0969-8051/

peptides, and small molecules that target a number of different antigens and receptors.

The tumour microenvironment is characterized by interstitial hypertension, hypoxia, low extracellular pH, decreased lymphatics, and the angiogenesis of blood vessels with defective architecture [3,4]. These abnormalities result in the leakage of blood plasma components into tumour tissue, where they are then retained. The latter explains why certain macromolecular drugs (>40 kDa for the renal excretion threshold [5]) preferentially accumulate within the tumour, a phenomenon noted by Matsamura and Maeda and termed the "enhanced permeability and retention (EPR) effect" [6]. New cancer diagnostics or therapeutics can be also be designed to exploit the tumour microenvironment and the EPR effect ('passive' targeting) [7,8]. Passive targeting agents include polymers, liposomes, nanoparticles, and some larger proteins. Active and passive targeting can be used in combination to improve the efficacy of drug delivery to the tumour site and uptake by the cancer cells.

A theranostic radiopharmaceutical contains a radionuclide and can provide both a diagnostic as well as a therapeutic option depending on the radioisotope that is coordinated to it [9]. The design of a targeted theranostic radiopharmaceutical for oncological purposes requires careful consideration of the physical decay properties of the radioisotope to be used, the specific *in vivo* targeting mechanism for the tumour and the clearance of the compound from other tissues so that the radioisotope, the targeting molecule, the chelating agent and the linker are all compatible with each other for maximum *in vivo* stability [10]. Taking these factors into consideration, the general aim of this project was therefore to develop a new dual-target bioconjugate greater than 40 kDa in size that could be radiolabelled with a therapeutic or a diagnostic isotope for potential theranostic purposes.

The diagnostic isotope selected was copper-64 ($t_{1/2} = 12.7$ h), which decays though positron emission (17%, 655 keV), electron capture/Auger-emissions (44%) and beta emission (39%, 573 keV) [11,12]. Copper-64 and its other isotopes (^{60}Cu, ^{61}Cu, ^{62}Cu, ^{67}Cu) have been shown to complex to many chelating agents with high stability and have been used in many radiopharmaceutical applications [11–15]. While copper-64 and the other copper isotopes are mostly used for diagnostic purposes, copper-67 ($t_{1/2} = 61.8$ h) emits beta (β^-) particles of 580 keV (100%) (penetration range of 2.1 mm) with gamma rays of 92 and 184 keV being useful for therapeutic applications. Copper-64 and copper-67 together form a theranostic isotope pair that can be used for diagnosis and therapy [12,16]. This ^{64}Cu/^{67}Cu-theranostic is a favourable option for a theranostic agent, however, the limitation with using copper-67 is its high production cost and limited availability. Recently, copper-64 has been investigated as a single theranostic isotope for both its proven diagnostic use and potential therapeutic capabilities (beta and Auger-emissions), however use as a therapeutic isotope is limited by the high dosage required to achieve therapeutic value [11].

The compound proposed for development as a potential theranostic radioligand is shown in Fig. 1 and was designed to attach to a larger passive targeting agent such as albumin to form a bioconjugate. This ligand will be referred to as GluCAB (Glucose-Chelator-Albumin-binder). GluCAB-maleimide-**1** (**1**) comprises a distally *N*-di-functionalised cyclam chelating agent, functionalised through sequential *N*-alkylation with a glucose moiety and a maleimide, each contained at the end of a polymethylene linker, as well as two carboxymethylene groups at the other cyclam nitrogens for radionuclide coordination and stability. This ligand is theoretically capable of being labelled with a radionuclide, and thereafter, the expectation was that the covalent addition of circulating, endogenous human serum albumin (HSA) [17] to the maleimide *via* Michael addition of a cysteine thiol group, would furnish the active bioconjugate.

The protein carrier and passive targeting agent selected, human serum albumin (HSA), has a molecular weight of 66.5 kDa (large enough for the EPR effect), is the most abundant serum protein (35–50 g/L, 50–60%), and has a half-life of around 19 days, making it very stable in context [18,19]. HSA has been used as a protein carrier in the development of new targeting agents [17], such as FDA-approved Abraxane (paclitaxel-albumin nanoparticle) for the treatment of breast cancer [20]; and for improving the biological half-life, pharmacokinetics and overall therapeutic efficacy of radiopharmaceuticals, such as ^{177}Lu-DOTA-TATE and ^{177}Lu-PSMA [21–23]. Small molecule binding to albumin can either be covalent – a Michael addition of the thiol of cysteine-34 to a maleimide [17,19,21] – or reversible, non-covalent – physical interactions of 4-(*p*-iodophenyl)butyric acid and Evans Blue (azo dye) with the protein [22].

Adding a glucose moiety to the molecule can be pharmacologically advantageous; firstly, the glucose increases the hydrophilicity and therefore the aqueous solubility of the ligand and secondly, it plays a supportive role as an active targeting agent on a cellular level. The concept of conjugating glucose as the active targeting agent was based on the well-known expression of glucose transporters (GLUT) on the cell surface, and up-regulation on most cancer cells owing to their high glucose requirement for provision of energy and metabolic needs [24,25]. The most widely used radiopharmaceutical that exploits this property for cancer diagnosis is [^{18}F]Fluorodeoxyglucose ([^{18}F]FDG) [26] and based on this same principle of GLUT and glycolysis targeting, a few other glucose analogue targeting agents have also been developed [27–30]. Most recently, a glucose-targeted probe (1380 g/mol) for photoacoustic and fluorescent imaging was proven to have cell uptake through GLUT [31].

For the GluCAB design the tetra-amine macrocycle *cyclam* was identified as the chelating agent as it is cheap and readily available and cyclam derivatives have been widely used for the complexation of a number of different metals with very good *in vivo* stability for a range of medicinal applications [32–35]; with furthermore, these cyclam derivatives are often used as the chelator of choice for complexation of copper-64 for PET imaging purposes.

The development of GluCAB as a new targeted ^{64}Cu/^{67}Cu-radioligand for potential theranostic applications was planned in a phased approach. The first phase encompassed the ligand synthesis and radiolabelling while the subsequent phases would involve *in vitro* stability along with *in vivo* metabolism in healthy animals (phase 2), and *in vivo* tumour targeting in a xenograft animal model (phase 3). Herein is described the synthesis of the desired GluCAB-maleimide-**1** followed by techniques for radiolabelling of this compound with copper-64 (phase 1). In addition, phase 2, for a preliminary understanding of the *in vivo* characteristics of [^{64}Cu]Cu-GluCAB-maleimide-**1** and its albumin-binding potential, is also reported through the use of small animal PET/CT imaging followed by *post mortem* biodistribution.

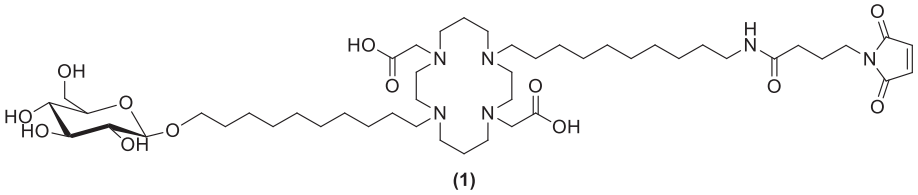

(1)

Fig. 1. The structure of GluCAB-maleimide-**1**.

2. Results and discussion

GluCAB-maleimide-**1** was synthesised according to the retrosynthetic analysis shown in Scheme 1. The synthesis required the sequential *N*-alkylation of di-(*tert*-butyl acetate) cyclam (**5**) using tethered glycosyl bromide (**4**) (active targeting moiety) followed by Boc-protected amine (**6**) as functionalised linkers and subsequent functional group inter-conversions, and will be discussed in the text. The preferred order of alkylation between linkers (**4** and **6**) and the challenges faced during synthesis will further be discussed.

2.1. Synthesis of linkers

Synthesis of the C-1, *O*-alkylated glycosyl bromide (**4**) is shown in Scheme 2A. It involved using the one-pot glycosylation method of Murakami et al. [36] in which perbenzoylated glucose (**8**) was converted, almost exclusively, to its α-glycosyl iodide (**9**) using iodine and hexamethyldisilazane (*in situ* producer of iodotrimethylsilane (Me_3SiI)) under Lewis acid catalysis with zinc chloride. The formation of the glycosyl iodide α-anomer using Me_3SiI has been previously proven and studied mechanistically [37]. Iodide (**9**) was not purified but substituted directly with 10-bromodecanol *via* activation with 1 eq. of $ZnCl_2$ to form the β-anomer of glycoside (**4**) (59% yield over the two steps).

The β-glycoside (**4**) formed diastereoselectively *via* exclusive β-addition of 10-bromodecanol onto the intermediate oxocarbenium ion (from iodide ionization with the Lewis acid $ZnCl_2$), due to neighbouring group participation by the 2-benzoyl group on the α-face. A C-10 alkyl chain was used for the linker in order to minimize steric interference between the targeting agent-chelator and the biomolecule carrier (albumin) during biological targeting. In a previous study that investigated the effects of the linkers of albumin-binding compounds on the *in vitro* and *in vivo* properties, it was found that an alkyl linker performed slightly better than a larger, more hydrophilic PEG linker [38]. The synthesis of the second linker, Boc-protected amine (**6**), for alkylative attachment to the chelator, was achieved according to a series of standard functional group conversion reactions as indicated in Scheme 2B. 10-amino-1-decanol (**11**) was obtained through a Gabriel reaction by first treatment of 10-bromo-1-decanol with potassium phthalimide followed by subsequent hydrolysis of the phthalimide (**10**) formed with hydrazine hydrate. The resultant amine was then protected as a *t*-butyl carbamate (**12**) followed by conversion of the hydroxyl group to bromide (**6**) under Appel conditions. The yields of each step were high (>85%) throughout.

2.2. Functionalisation of cyclam

Distal, sequential dialkylation of cyclam (**5**) with bromide-linkers (**4**) and (**6**) required prior protection of two of the distal nitrogens of cyclam with alkoxycarbonylmethylene groups. However, alkylation studies with *t*-butyl bromoacetate and a base resulted in a complex mixture containing six alkylated cyclam compounds, amongst which were three difunctionalised regioisomers that included the desired 1,8-*N*,*N*′-di-functionalised product. The ratio of mono, di and trisubstituted prod-

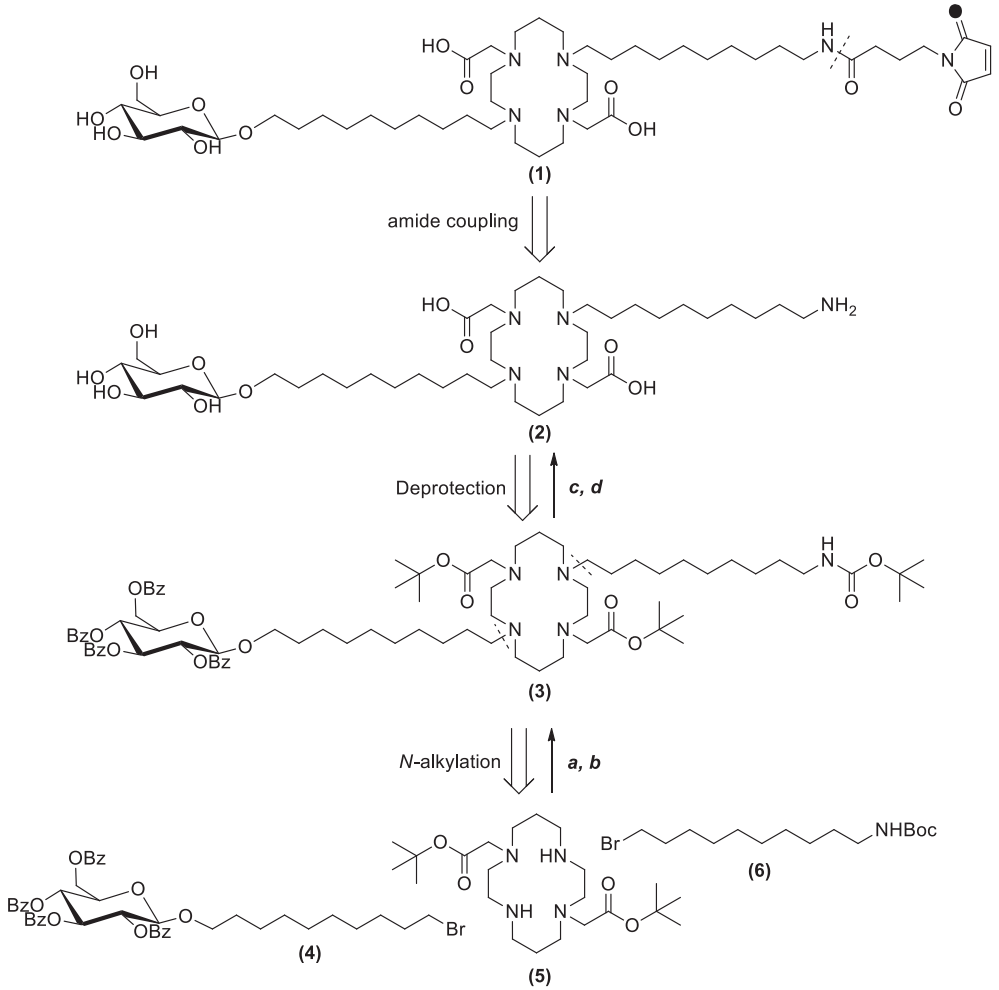

Scheme 1. Retrosynthetic analysis of GluCAB-maleimide-**1** and the synthesis of GluCAB-amine-**2** (a) Glycosyl bromide (**4**), K_2CO_3, MeCN, 60 °C, 16 h (58%), (b) carbamate (**6**), K_2CO_3, MeCN, 80 °C, 16 h (74%), (c) NaOMe, MeOH, 1 h (71%), (d) TFA:CH_2Cl_2 (1:1), 16 h (69%)

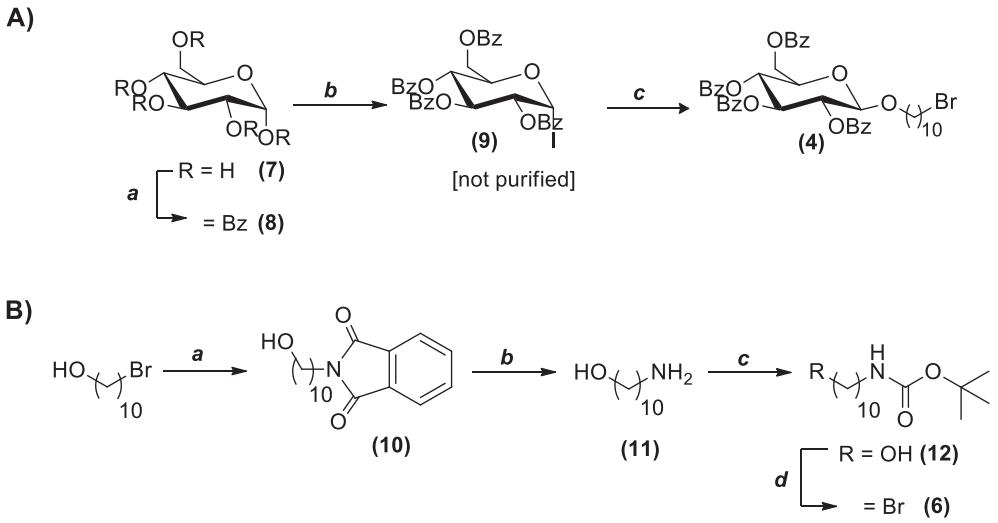

Scheme 2. Synthesis of linkers - glycosyl bromide (**4**) and Boc-protected amine (**6**) **A**) (a) BzCl, pyridine, 0 °C – RT, (89%), (b) I_2, $(Me_3Si)_2$, $ZnCl_2$, CH_2Cl_2, 16 h, RT (c) 10-bromodecanol, $ZnCl_2$, Molecular sieves 4 Å, CH_2Cl_2 (59% over steps a and b). **B**) (a) Potassium phthalimide, DMF, 100 °C, 20 h, (97%) (b) Hydrazine hydrate, EtOH, reflux, 24 h (88%), (c) $(Boc)_2O$, DCM:MeOH 4:1, 3 h, (89%), (d) CBr_4, PPh_3, DCM, (92%)

ucts could be slightly manipulated by adjusting the equivalents of *t*-butyl bromoacetate but a mix of the products was still obtained. The maximum amount of disubstituted product could be obtained by the addition of 3 equivalents of the *t*-butyl bromoacetate over 6 h in increments of 0.5, using potassium carbonate as base (2.5 equiv). These three regioisomers could, with difficulty, then be purified from each other using column chromatography (CH_2Cl_2:MeOH 5:1), but the yield of each (1,4-*N*,*N*′ = 16%; 1,8-*N*,*N*′ = 41%; 1,11-*N*,*N*′ = not determined) was very low.

A method developed by Pandya et al. [39] (Scheme 3) reported the selective synthesis of cyclam (**5**) starting from 1,4,8,11-tetraazatricyclo [9.3.1.1^{4,8}]hexadecane (tricyclic bis-aminal cyclam (**13**)) *via* a quaternary ammonium salt intermediate. Cyclam (**13**), synthesised by alkylation of cyclam with formaldehyde (2 eq), comprises the bridging of two of the six-membered rings in cyclam as aminals in stable chair conformations, which makes the outward-facing lone pairs more available for alkylation (at positions 1 and 8). Following quaternization, the methylene bridges are base-hydrolysed to afford symmetrical *trans*-disubstituted cyclam (**5**).

Following the method [39] as described for the alkylation of (**13**) to form (**5**), the product isolated proved rather to be the mono-alkylated cyclam (**14**) (65% yield) in which the aminal bridge at the site of alkylation was deprotected *in situ* as a result of water present in the reaction (originating from crystal structure of recrystallized (**13**)) *via* the mechanism proposed in Supporting Information Scheme S1. This reaction was repeated numerous times with similar results and could therefore represent a novel method for mono-alkylation of a cyclam macrocycle. 1,8-*N*,*N*′-disubstituted cyclam (**5**) was then obtained by reacting (**13**) with excess t-butyl bromoacetate (6 eq) in acetonitrile for 5 days at 70 °C and precipitation of a crude product with diethyl ether. The 1,8-*N*,*N*′-disubstituted cyclam (**5**) was recrystallized from acetonitrile with a small percentage (<5%) of methanol in a 20% yield. The ^{1}H and ^{13}C NMR spectral data (see Supporting Information Fig. S1) was in accordance with that reported in the literature for a 1,8-*N*,*N*′-disubstituted cyclam [40]. Briefly, ^{1}H NMR indicated the required peaks for the cyclam macrocycle and the two *t*-butyloxycarbonylmethylene groups distally: one methylene singlet (4H, 3.30 ppm); one t-butyl group (18H, 1.43 ppm); multiplets at 1.72 ppm (4H), 2.60 ppm (4H), 2.69 ppm (8H) and 2.74 ppm (4H) for the symmetrically equivalent methylene groups of a distally disubstituted cyclam macrocycle. Similarly, ^{13}C data showed only 5 cyclam resonances. The data for 1,8-*N*,*N*′-cyclam (**5**) was also distinguishable [40] from the previously isolated and identified 1,4-*N*,*N*′-regioisomer (see Supporting Information, Fig. S2), as well as the 1,11-isomer, based on symmetry considerations. Although low-yielding, this procedure was found to be reproducible, furnished high-purity (**5**) and could be scaled up. GluCAB-amine-**2** was then synthesised *via* standard alkylation and deprotection strategies as shown in Scheme 1.

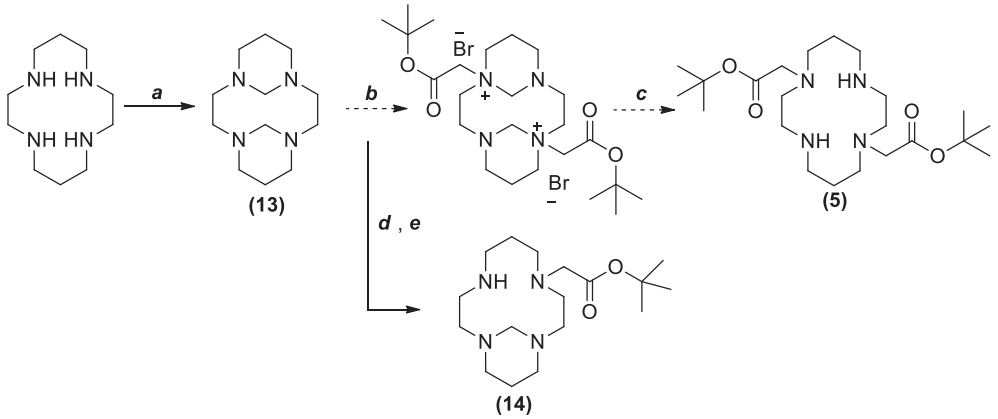

Scheme 3. Selective synthesis of *trans*-disubstituted cyclam (**5**) according to Pandya et al. [39] (a) Formaldehyde (2 eq), H_2O, RT, 2 h (b) $BrCH_2CO_2^t$-Bu (4 eq), MeCN, 60 °C, 24 h (c) 3 M NaOH, RT, 3 h and the mono-alkylated cyclam (**14**) obtained (d) $BrCH_2CO_2^t$-Bu (4 eq), MeCN, 60 °C, 48 h, (e) 3 M NaOH, 16 h, (65%)

Briefly, cyclam (**5**) was alkylated using glycoside (**4**) (0.45 eq – limiting reagent to minimize formation of di-glycosylated product) to form mono-glycosylated cyclam (**15**) (58%) (full synthesis in Supporting Information), followed by alkylation using carbamate (**6**) (2.0 eq) to yield cyclam (**3**) (74%). Both alkylations used potassium carbonate (3.0 eq) in acetonitrile with heating (60 or 80 °C) for 16 h. Alkylation with glycoside (**4**) was performed first so as to introduce UV activity into the structure, which assisted with chromatography and isolation. Similarly, the order of deprotecting the protecting groups of cyclam (**3**) (benzoate esters, *tert*-butyl esters and *tert*-butyl carbamate) was completed in a way that ensured the easiest purification. Deprotection of the benzoate esters of (**3**) to yield cyclam (**16**) (Supporting Information) was completed under nucleophilic conditions using sodium methoxide, towards which the *tert*-butyl esters and carbamate were stable. Compound (**16**) could be purified using silica-based column chromatography. Further Boc- and *tert*-butyl ester deprotection of (**16**) was carried out under acidic conditions using TFA to afford GluCAB-amine-**2** (**2**), for which full characterisation was carried out (see the Supporting Information). The glycosyl functionality of GluCAB-amine-**2** was found to be stable under the acidic Boc-deprotection conditions using TFA, in which only a very small amount (<10%) of by-product was fortunately observed. The purification of free GluCAB-amine-**2** using column chromatography (silica gel 60, DCM:MeOH:NH_4OH 7:2.5:0.5), however, proved challenging as a result of polarity, which caused the compound to adhere to the stationary phase. Consequently, while the reaction conversion seemed high (~90% according to TLC), the reaction yield was fairly low (<50%). The stationary phase was then changed to an Alumina-N matrix in which elution with DCM:MeOH:NH_4OH (8:1.7:0.3; 7:2.5:0.5; 6.5:3:0.5) removed the impurities, after which the product could be eluted with 40% H_2O in MeOH. Once concentrated, the product was desalted on a solid phase extraction (SPE) C18 light cartridge using water, and eluted from the cartridge using 50% MeOH in H_2O. The product was dried under an air stream, re-dissolved in water (1 mL), frozen and lyophilised to yield a colourless solid powder pellet. The yield of GluCAB-amine-**2** obtained from this purification was improved to 69%, leading to an overall yield, over the four steps from cyclam **5**, of 21%.

Insertion of the two linkers in the *N*4 and the *N*11 position of GluCAB-amine-**2** ensured placement of the glucose targeting moiety distally away from the albumin carrier (that would eventually be attached to the terminal amine position) allowing for minimal interference between the two positions. This structure also placed the two coordinating carboxylic acid groups opposite to each other to form a more stable, octahedral type geometry when coordinating the radioisotope [40].

2.3. Maleimide insertion

The concept of a GluCAB bioconjugate requires the *in vivo* binding of the synthesised ligand to albumin. Towards this end the primary amine of GluCAB-amine-**2** was converted into a maleimide (GluCAB-maleimide-**1**), thereby providing a Michael acceptor for capture of the free Cys-34 thiol group of albumin as described previously [17,19,21]. GluCAB-maleimide-**1** was synthesised through a mixed anhydride peptide coupling strategy in which 4-maleimidobutyric acid NHS-ester (**18**) (synthesised from 4-maleimidobutyric acid (**17**)) (Scheme 4) dissolved in DMF was reacted with GluCAB-amine-**2** in an aqueous medium (model reactions and different peptide coupling strategies are displayed in Supporting Information Schemes S2 and S3). The advantage of this NHS-coupling method over other mixed anhydride methods was that the aqueous medium was more suitable for miscibility and reaction of the highly polar GluCAB-amine-**2**. However, equally, this method suffered from sensitivity of the NHS-ester (**18**) towards hydrolysis in an aqueous medium, especially at an acidic (pH < 7) or basic pH (pH > 8). The NHS-ester (**18**) was found to be most stable when dis-

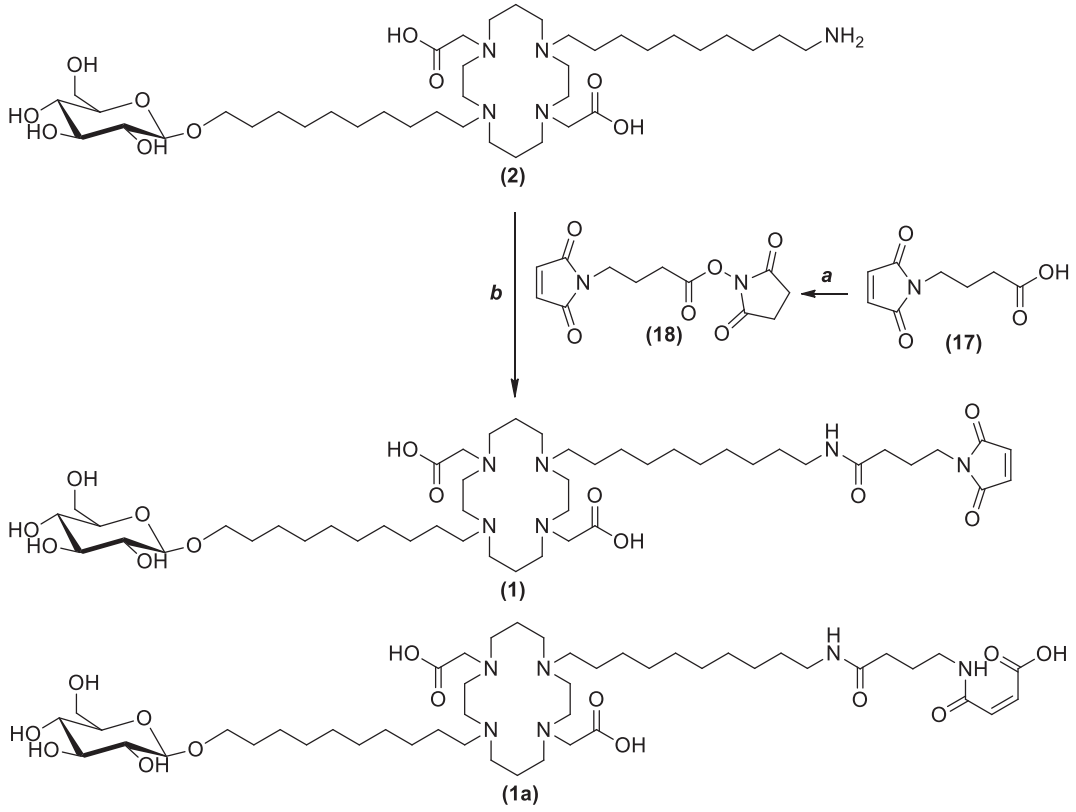

Scheme 4. Synthesis of GluCAB-maleimide-**1** (a) NHS, DIC, DCM, 2 h, RT (72%) (b) 0.01 M PBS, pH 7.4, 1 h, RT (55%) (mz[+H] = 955.6) (hydrolysed maleamic acid product 1a (mz[+H] = 973.6)).

solved in an organic solvent, which resulted in optimized reaction conditions involving the addition of small increments of the NHS-ester in DMF to the amine in a 0.01 M PBS buffer (pH 7.4) at room temperature.

The conversion from starting material (GluCAB-amine-**2**) to a single product (GluCAB-maleimide-**1**) could be observed on TLC. This product was very soluble in water because of its high polarity and needed to be purified using a Sep-Pak C-18 Plus light cartridge as described in the methods. During purification, it appeared that some of the maleimide product was degrading (hydrolysing) and only approximately 50% of GluCAB-maleimide-**1** product was isolated. HPLC-MS analysis of (**1**) after 1 h in water indicated two peaks (8.5 and 9.0 min) in the UV-trace (210 nm). The 8.5 min peak ($mz[+H] = 973.6$) proved to be the maleamic acid compound (**1a**) (Scheme 4) while the 9.0 min peak ($mz[+H] = 955.6$) corresponded to the GluCAB-maleimide-**1**.

Overall, the maleimide functionality proved to be very sensitive towards hydrolysis to the open maleamic acid form, especially under acidic conditions (pH < 6.5), at higher temperatures, and in the presence of nucleophiles. This sensitivity, therefore, had to be carefully considered during any proposed radioisotope complexation, as maleimide hydrolysis during this process and subsequent administration of the maleamic acid compound *in vivo* was feared would have a serious effect on the compound's biological efficacy due to inefficient albumin-binding.

2.4. Radiolabelling

2.4.1. Preparation of [^{64}Cu]$CuCl_2$ and radiolabelling of GluCAB-amine-2

Copper-64 was obtained through irradiation of natural CuO (69.17% abundance of ^{63}Cu) in the SAFARI-1 research reactor at Pelindaba, Necsa *via* the ^{63}Cu(n,γ)^{64}Cu nuclear reaction [41]. This method produces copper-64 of a lower specific activity as compared to the more widely used method of enriched ^{64}Ni-target irradiation with low energy protons (11–14 MeV; ^{64}Ni(p, n)^{64}Cu) [42,43] but it is less expensive and more easily accessible than the cyclotron-produced copper-64. A [^{64}Cu]$CuCl_2$ solution was prepared with a specific (molar) activity of 1450 GBq/g (115 MBq/μmol).

As previously mentioned copper-64 is known to form kinetically inert and thermodynamically stable complexes with a variety of cyclam chelators. These complexes form under a wide range of reaction conditions that need to be compatible with the functional groups attached to the macrocycle. Earlier, we had established that the maleimide functionality of GluCAB-maleimide-**1** had revealed a high sensitivity towards hydrolysis under acid conditions and in aqueous solutions at high temperatures. Therefore, in pursuit of the ^{64}Cu-labelled GluCAB radioligand, complexation of GluCAB-amine-**2** with copper-64 was investigated to first determine optimal conditions, with the possible intention to incorporate the maleimide subsequently.

To this end, GluCAB-amine-**2** was reacted with the prepared [^{64}Cu]$CuCl_2$ (115 MBq/μmol; 0.33 eq) in a 0.1 M NH_4OAc solution at different pH's, temperatures, and incubation times. An overview of the experimental series is given in the Supporting Information Table S1. The best labelling efficiency (LE) for complexation of GluCAB-amine-**2** with copper-64 was found to be 98% with an average LE of 95% under the same conditions (pH 3.5; 95 °C; 30 min) irrespective of radioisotopic activity concentration. Radio-HPLC analysis of the reaction indicated that the free [^{64}Cu]$CuCl_2$ was only minimally retained on the reverse-phase HPLC column, eluting with a retention time of 3–4 min, while the slightly less hydrophilic [^{64}Cu]Cu-GluCAB-amine-**2** eluted at around 11.5 min. The LE decreased significantly ($p < 0.05$) upon incubation at higher pH values (pH 5 (86%) and 9 (80%)), for shorter reaction times (20 min (61%) and 10 min (39%)) or at lower temperatures (45 °C (5%), 70 °C (29%) or 80 °C (81%)).

The temperature of the reaction had the most detrimental impact on the radiolabelling since at 45 °C hardly any complexation occurred (<5% LE). Copper (II) is a medium hard/soft Lewis acid and forms strong bonds with the nitrogen of amino groups of macrocycles such as those in cyclam, especially when there are carboxylate pendant arms [33,34]. The formation of these bonds; however, requires a large amount of energy for the metal ion to overcome its kinetic inertness and bind to the N- and O-donors with dissociation from its chloride ligands to form an octahedral complex [44]. The temperature, therefore, is crucial for providing enthalpy of activation. The pH of the reaction also had a slight effect on complex formation in which the best complexation was observed at pH 3.5, while at pH 9 the LE decreased by 15%. A possible reason for this is that at the higher pH values, there are more negatively charged ions present in the reaction solution to compete for the positively charged copper ions, making the binding rate to the macrocycle slower and less efficient.

These optimized conditions (high temperature and low pH) for radiolabelling of GluCAB-amine-**2** with copper-64 preclude complex formation using GluCAB-maleimide-**1** because of incompatibility with the maleimide functional group. The maleimide incorporation using NHS-ester (**18**) as described, would therefore need to occur post-labelling.

2.4.2. Post-labelling conversion of [^{64}Cu]Cu-GluCAB-amine-2 to [^{64}Cu]Cu-GluCAB-maleimide-1

[^{64}Cu]Cu-GluCAB-amine-**2** was converted to [^{64}Cu]Cu-GluCAB-maleimide-**1** by reaction with a 4-maleimidobutyric acid NHS-ester (**18**) for 1 h in 0.01 M PBS at pH 7.4 and an incubation temperature of 40 °C. Pleasingly, the maleimide product (retention time = 13.5 min; 90% radiochemical purity; conversion of 93%) proved to be stable in the PBS buffer during the reaction process with no noticeable hydrolysis of the maleimide to the maleamic acid (retention time = 12.5 min) (Fig. 2). The UV-VIS retention time of the cold copper complexes matched the retention time of the radiolabelled complexes (data not shown). The time required for the reaction and purification (~1.5–2 h) was sufficiently lower than the half-life of copper-64 (12.7 h); thus, the process was suitable for a post-labelling conversion.

2.5. In vitro studies

2.5.1. Stability studies and protein binding of [^{64}Cu]Cu-GluCAB-amine-2 and [^{64}Cu]Cu-GluCAB-maleimide-1

Preliminary stability studies in 0.01 M PBS buffer were performed, firstly to test the tendency of the maleimide towards hydrolysis and secondly, to establish whether copper was lost from the chelator. For [^{64}Cu]Cu-GluCAB-maleimide-**1**, it was found that approximately 14% of the maleimide had hydrolysed after 24 h (0.01 M PBS (pH 7.4); room temperature) (Supporting Information, Fig. S3) with only a 1.5% re-occurrence in free copper-64 species.

Protein binding studies provide an indication of how well, if at all, a compound will bind to proteins in the blood, and especially to HSA, considering that this protein constitutes 60% of all serum proteins. Binding of the GluCAB compound to HSA was seen to be an essential part of the targeting mechanism and [^{64}Cu]Cu-GluCAB-maleimide-**1** was designed in such a manner (maleimide functionality) that a high percentage of protein binding was anticipated as reported in literature [19]. A protein binding study was carried out comparing [^{64}Cu]Cu-GluCAB-maleimide-**1** and [^{64}Cu]Cu-GluCAB-amine-**2** (no maleimide functionality), (Fig. 3). The radioactivity present in the proteins (precipitated and centrifuged out from serum) was measured following incubation (0, 1, 2 and 24 h) with each compound at 37 °C. Upon addition to the serum, [^{64}Cu]Cu-GluCAB-maleimide-**1** was immediately 85% protein bound which further increased to a maximum of 90% within 2 h that was sustained through to 24 h. The small percentage that remained 'unbound' could be attributed to the nature of the radiolabelling process in which 3% radioactivity remained as free [^{64}Cu]$CuCl_2$ and the residual as GluCAB-amine-**2**. Conversely, [^{64}Cu]Cu-GluCAB-amine-**2** showed a very low (30%) protein binding upon addition to the serum, which reached 50% protein binding after 24 h. This can be considered non-specific protein association, as no maleimide group was present. Possible non-specific interactions included charge interactions (between

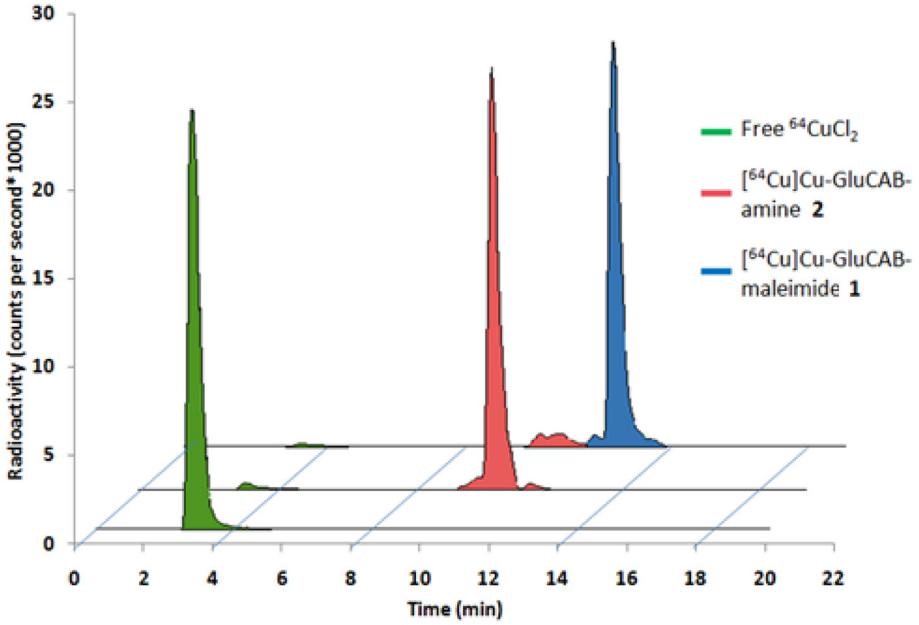

Fig. 2. Radio-HPLC chromatograms of free [^{64}Cu]$CuCl_2$ (green peak – RT = 3.4 min); [^{64}Cu]Cu-GluCAB-amine-**2** (pink peak – RT = 11.5 min; 97% radiochemical purity) and post labeling conversion to [^{64}Cu]Cu-GluCAB-maleimide-**1** (blue peak – RT = 13.5 min; 90% radiochemical purity, 93% conversion).

the protonated amino group and carboxylic acid functionalities), hydrogen bonding, and other hydrophobic interactions (between ligand and serum protein).

Serum stability studies were completed for both the [^{64}Cu]Cu-GluCAB-maleimide-**1** and the [^{64}Cu]Cu-GluCAB-amine-**2**. Radio-HPLC analysis seemed to indicate high stability of both ^{64}Cu-complexes to de-metallation as well as ligand robustness at 37 °C over the 24 h since no degradation products or increase in the amount of free copper-64 was observed (Supporting Information, Fig. S4).

A concern however, regarding the % protein binding noted for GluCAB-amine-**2** and the stability of the complexes as determined by absence of free copper-64, is the possible release of copper ions from the cyclam chelator with transchelation and binding of the copper to other serum proteins. Zarschler et al. [45] defined this challenge and sought to establish *in vitro* assays for determining the *in vivo* stability of Copper-64 macrocyclic complexes. This study noted that ^{64}Cu-labelled macrocycles (TETA, NOTA, DOTA, cyclam) exhibited very good complex stability with only 1.7–4.2% transchelation to serum proteins but a [^{64}Cu]Cu-NOTA conjugated to a single-domain antibody indicated 40% transchelation. The resistance to transchelation noted for the cyclam macrocyles indicates that the % protein binding noted for the ^{64}Cu-GluCAB complexes should be as a result of the maleimide group and some non-specific protein association, as indicated, with minimal copper released; however, the increase of transchelation upon conjugation of the copper-complex to a biomolecule warrants further investigation into the kinetic stability of the GluCAB complexes *in vivo*. [^{64}Cu]Cu-TETA which indicated high serum stability and low protein binding (4.2 ± 2.3% resistance to serum protein transchelation) [45] is to be used as a negative control for *in vivo* studies as this has been proven to be rapidly metabolised and cleared *in vivo* [46].

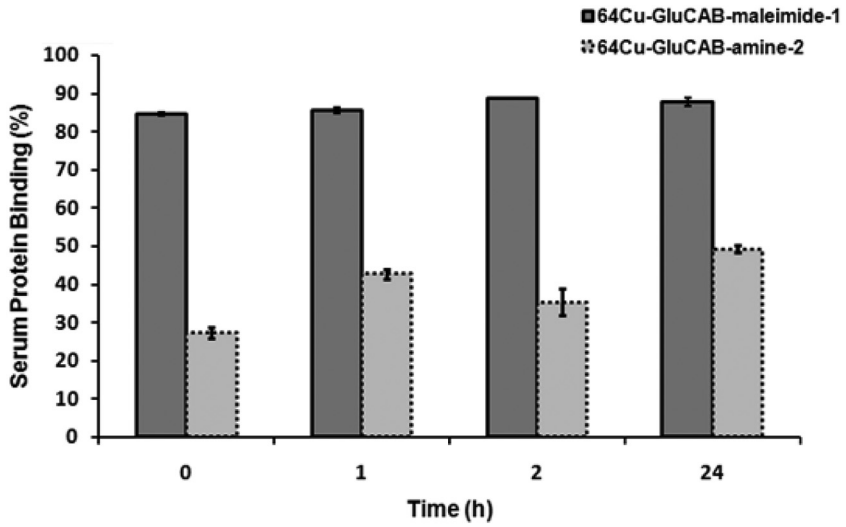

Fig. 3. Percentage binding of [^{64}Cu]Cu-GluCAB-maleimide-**1** and [^{64}Cu]Cu-GluCAB-amine-**2** to proteins in serum over a 24 h period at 37 °C (mean ± SD; $n = 3$).

2.6. In vivo studies

2.6.1. MicroPET/CT imaging studies in healthy Balb/c mice

The prospective capability of GluCAB for tumour targeting can only be evaluated *in vivo* since the first mechanism of uptake relies on binding of the GluCAB-maleimide-**1** to albumin and extravasation into the tumour through the EPR effect, which necessitates a living biological system. Valuable understanding of the tracer administration, metabolism, excretion and biodistribution of the compound needed to be achieved before further actual tumour targeting studies in mice could be attempted. This concept of altered biodistribution of [^{64}Cu]Cu-GluCAB-maleimide-**1** (and consequently the GluCAB bioconjugate) was therefore determined in healthy Balb/c mice using microPET/CT imaging followed by *post mortem* radioanalysis of excised organs and tissue. This was compared to the behavior of two other compounds; [^{64}Cu]Cu-TETA (negative control since rapid metabolism and excretion was anticipated) and [^{64}Cu]Cu-GluCAB-amine-**2** (lacking the maleimide functionality; predicting a faster excretion rate despite non-specific serum protein binding). Similar compound concentrations of [^{64}Cu]Cu-TETA (100 μL; 1.2 ± 0.22 MBq; 39 nmol/mouse), [^{64}Cu]Cu-GluCAB-amine-**2** (150 μL; 5.6 MBq, 31 nmol/mouse) and [^{64}Cu]Cu-GluCAB-maleimide-**1** (100 μL; 1.0 ± 0.09 MBq, 31 nmol/mouse) were administered for comparison of the groups ($n = 5$); no adverse side effects were noted. Subsequently, microPET/CT imaging was conducted over a 24 h period for which maximum intensity projection (MIP) allowed for a visual comparison between the biodistribution of the three compounds (Fig. 4).

The MIP images represent the expected [^{64}Cu]Cu-TETA biodistribution (Fig. 4A) as reported in literature [46], which is dominated by a rapid tracer clearance from the blood pool and a major systemic clearance by way of renal excretion (*i.e.* high activity present only in the bladder within 1–2 h post injection). Furthermore, at 24 h post-injection (p.i), only minimal activity was still evident in the animal. By comparison, the [^{64}Cu]Cu-GluCAB-amine-**2** microPET/CT (Fig. 4B) visualised the occurrence of activity within the hepatobiliary system, suggesting a different route of excretion compared to [^{64}Cu]Cu-TETA. However; just as [^{64}Cu]Cu-TETA, [^{64}Cu]Cu-GluCAB-amine-**2** had cleared early-on in significant amounts and within 24 h p.i negligible radioactivity concentration in all major organs (except for intestines) was observed. MIP images of the mice administered with [^{64}Cu]Cu-GluCAB-maleimide-**1** (Fig. 4C) showed that this compound had a prolonged biological half-life and blood circulation as indicated by the high overall systemic activity (a blue colour in the image) and clear visibility of the heart even at 8 h p.i as compared to [^{64}Cu]Cu-GluCAB-amine-**2**. These images also clearly indicated a high accumulation of radioactivity in the liver, intestines, and bladder from 1 to 8 h p.i. This activity was mostly cleared after 24 h but with some hepatic radioactivity activity still notable.

Further analyses included the image-guided quantification from volumes-of-interest (VOI), yielding standard uptake values (SUV (g/mL)); *e.g.* VOI and SUV indicative of the decay-corrected compound concentration in the heart muscle (representing blood pool) for each time point, allowing for an estimation of their biological half-life. The heart activity concerning [^{64}Cu]Cu-TETA and [^{64}Cu]Cu-GluCAB-amine-**2** calculated from the 1 h PET image was 0.02 and 0.04 g/mL, respectively. This was deemed fairly low and reflected the representation from the images. Therefore, the biological half-lives of these two compounds were assumed to be <5 min, but could not be exactly determined. However, analysis of the heart region for [^{64}Cu]Cu-GluCAB-maleimide-**1** (1 h = 1.44 g/mL) indicated the expected exponential decrease of the circulating activity over the 24 h period (24 h = 0.10 g/mL) and estimated the biological half-life as about 6–8 h. Other notable SUV for [^{64}Cu]Cu-GluCAB-maleimide-**1** included the liver (max. 2.74 g/mL at 1 h to min. 0.29 g/mL at 24 h) and intestines (max. 0.79 g/mL at 4 h to min. 0.07 g/mL at 24 h).

According to current theories [47] on drug metabolism, the most common routes of drug elimination is renal excretion (glomerular filtration of small, hydrophilic, non-protein bound drugs or tubular secretion of larger, protein-bound drugs); or hepatobiliary excretion (more lipophilic compounds). In the study of the metabolism and excretion of drug-radioisotope complexes, it has been noted that the clearance pathway, specifically of bifunctional chelate conjugates, is significantly influenced by the lipophilicity and net charge of the complex [46]. The more lipophilic a complex is the higher the liver accumulation will be and the slower the systemic clearance. Similarly, a conjugate with a positively-charged complex exhibits slow excretion through the liver but conversely, a negatively-charged complex is more rapidly and efficiently cleared through the kidneys. The routes of excretion noted from the MIP PET images for all three compounds are in line with the above mentioned aspects on compound metabolism and excretion. [^{64}Cu]Cu-TETA is a relatively small, hydrophilic molecule with a net negative complex charge while [^{64}Cu]Cu-GluCAB-maleimide-**1** and [^{64}Cu]Cu-GluCAB-amine-**2** are more lipophilic with a neutral complex charge. As identified by the amount of activity in the specific organs involved with excretion (kidneys, bladder, liver, intestines), [^{64}Cu]Cu-TETA was excreted through the renal system while [^{64}Cu]Cu-GluCAB-maleimide-**1** and [^{64}Cu]Cu-GluCAB-amine-**2** were eliminated to different extents *via* the hepatobiliary system.

Although [^{64}Cu]Cu-TETA and [^{64}Cu]Cu-GluCAB-amine-**2** have similar blood clearance rates, the difference between their excretion can potentially be explained by: 1) the difference in molecular weight of the compounds (432.5 g/mol *versus* 790.1 g/mol) making the smaller TETA compound more suitable for rapid glomerular filtration; 2) the difference in charge between the two complexes (negative *versus* neutral), which influences the hydrophilicity of the compounds; 3) the tethers (C-10-aliphatic chains) attached to the chelator for [^{64}Cu]Cu-GluCAB-amine-**2** that renders this compound more lipophilic and therefore prone to hepatobiliary metabolism; and 4) the nominal non-specific binding of [^{64}Cu]Cu-GluCAB-amine-**2** to serum proteins (as herein determined) that may provoke more hepatic involvement.

Similar to [^{64}Cu]Cu-GluCAB-amine-**2**, [^{64}Cu]Cu-GluCAB-maleimide-**1**, is a lipophilic and neutrally charged complex that shows metabolism through the liver but with the difference of having a tethered maleimido functional group. This study confirmed a markedly prolonged biological half-life of [^{64}Cu]Cu-GluCAB-maleimide-**1** (6–8 h) compared to -amine-**2** (<5 min). This may be sufficient proof of the effectiveness of the maleimide functionality for binding to albumin and therefore substantially extending an unwanted-short tracer residence time in the blood circulation. The albumin-binding of [^{64}Cu]Cu-GluCAB-maleimide-**1** in turn affected the rate of liver metabolism, which seemed markedly reduced as inferred from the prolonged and high accumulation of activity in the liver and intestines over the 24 h period. The high activity seen in the liver could be enhanced by the prolonged plasma retention of the compound and the fact that the liver is a highly perfused organ but albumin is known to be eliminated through renal (6%), hepatobiliary (10%) and other catabolic (84%) mechanisms [48], and therefore the activity which was seen in the liver and intestines is not unexpected for a covalently bound GluCAB-albumin bioconjugate. While reversible albumin-binding [22] allows for a slow release and accumulation of the drug at the target site as a result of a longer circulation time, the release of the small molecule implies that renal excretion will mostly be evident. Covalent albumin-binding can both, improve on the drug circulation time as well as facilitate tumour delivery and retention there in through the EPR-effect [21] but the drug is not easily released and the excretion mechanism would be that of a larger, lipophilic construct through the liver.

The accumulation of activity in the liver of the [^{64}Cu]Cu-GluCAB-maleimide-**1** injected mice could also have been as a result of a few possible other processes: firstly, a loss of the copper(II) ions from the chelator complex in the blood stream followed by subsequent binding of the ionic copper to serum proteins and delivery to the liver for further

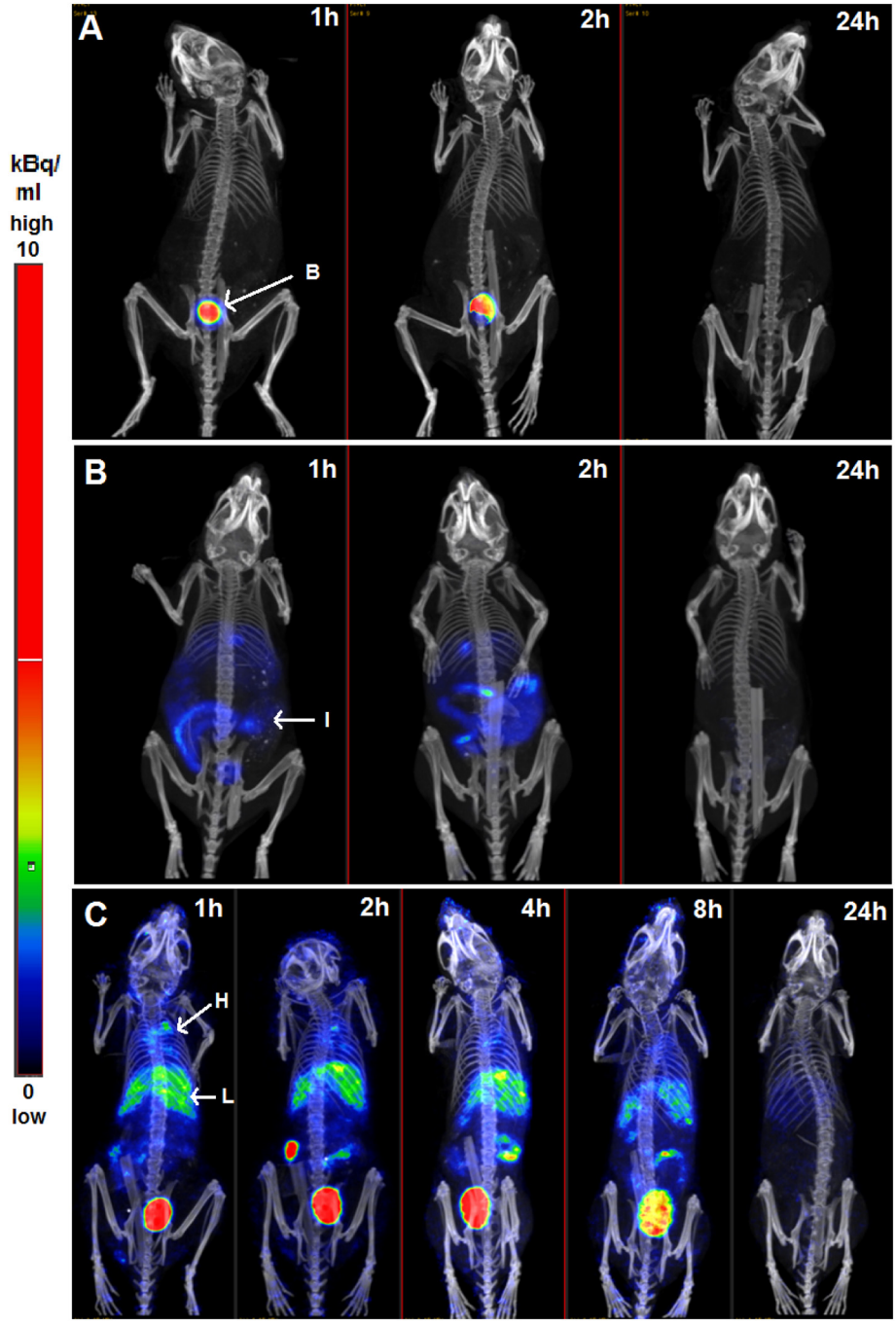

Fig. 4. Maximum intensity projection microPET/CT images (anterior view) of BALB/c mice following injection with (**A**) [^{64}Cu]Cu-TETA (100 μL; 1.2 ± 0.22 MBq; 39 nmol/mouse), (**B**) [^{64}Cu]Cu-GluCAB-amine-**2** (150 μL; 5.6 MBq, 31 nmol/mouse) and (**C**) [^{64}Cu]Cu-GluCAB-maleimide-**1** (100 μL; 1.0 ± 0.09 MBq, 31 nmol/mouse). Image acquisition was done under isoflurane anaesthesia (2%) at 1, 2 and 24 h (A/B) and at 1, 2, 4, 8 and 24 h (C) post injection (n = 3). (CT scan = 5 min; PET scan = 20 min); B = bladder; H = heart; L = liver; I = intestines. Normalised scale bar 0–10 kBq/mL.

processing; or secondly, but less likely, transchelation of the copper from the GluCAB complex to a copper-dependent enzyme, *e.g.*, superoxide dismutase (SOD), that is highly abundant in liver cells [45]. ^{64}Cu-labelled cyclam and TETA have been proven to show enhanced resistance to both serum protein and SOD transchelation [45]; however, it has also been noted that a chelator-biomolecule complex is less kinetically stable *in vivo* and therefore these processes and liver accumulation for [^{64}Cu]Cu-GluCAB-maleimide-**1** need to be further investigated.

2.6.2. Biodistribution studies

The image-guided quantification matched the illustrated distribution behavior of the compounds with the normalised organ activity concentration (SUV) for [^{64}Cu]Cu-TETA, [^{64}Cu]Cu-GluCAB-amine-**2** and [^{64}Cu]Cu-GluCAB-maleimide-**1** provided first such results. Following the last image acquisition, the *post mortem* biodistribution analysis quantifies the precise amount of radioactivity per organ allowing herein the robust comparison of the ^{64}Cu-labelled compounds as illustrated in Fig. 5.

As already indicative from 24 h MIP image in Fig. 4A, very low ^{64}Cu-activity amounts were obtained for [^{64}Cu]Cu-TETA; indeed all organs showed negligible TETA levels *ex vivo* (on average 0.20 ± 0.06%ID/g) with the only notable radioactivity found in the kidneys (0.37 and 0.40%ID/g). No notable difference between the activity in the organs of mice injected with [^{64}Cu]Cu-TETA and [^{64}Cu]Cu-GluCAB-amine-**2** was observed - except for a 6-fold higher [^{64}Cu]Cu-GluCAB-amine-**2**

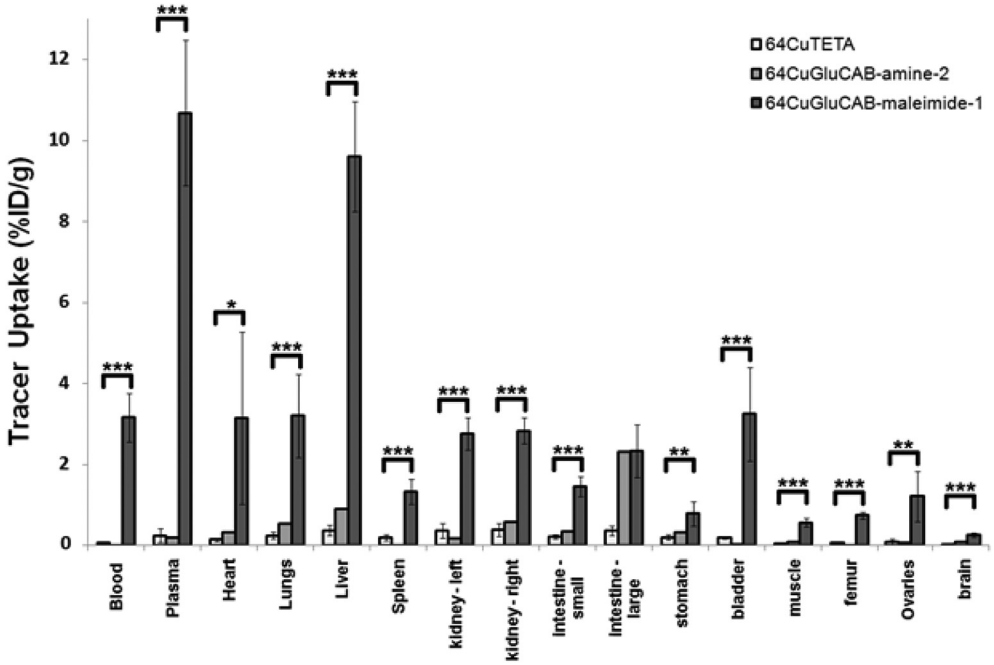

Fig. 5. Comparison of *ex vivo* biodistribution at 24 h after injection of [^{64}Cu]Cu-TETA (n = 5), [^{64}Cu]Cu-GluCAB-amine-**2** ($n = 1$) and [^{64}Cu]Cu-GluCAB-malemide-**1** (n = 5) presented as mean %ID/g ± SD; two-tailed Student's *t*-test comparing radiolabelled TETA with GluCAB-malemide-**1** returned $p < 0.05$ (*), $p < 0.01$ (**) or $p < 0.001$ (***).

presence within the large intestine (2.31%ID/g) and 2.5-fold higher [^{64}Cu]Cu-GluCAB-amine-**2** hepatic presence (0.91%ID/g). This confirms the excretion patterns and conclusions drawn from the microPET/CT image analysis. The [^{64}Cu]Cu-TETA and [^{64}Cu]Cu-GluCAB-amine-**2** compounds were rapidly eliminated from the system through the renal and hepatobiliary pathways, respectively. The biodistribution analysis of [^{64}Cu]Cu-GluCAB-maleimide-**1** mice recorded the maximum ^{64}Cu-activity in the plasma (10.7 ± 1.8%ID/g) and the liver (9.6 ± 1.4%ID/g) with the activity in all the other organs being <4%ID/g. Therefore, the activity of [^{64}Cu]Cu-GluCAB-maleimide-**1** in all the organs was significantly different ($p < 0.05$ or less) as compared to that of [^{64}Cu]Cu-TETA and [^{64}Cu]Cu-GluCAB-amine-**2** except for the large intestines indicating similar [^{64}Cu]Cu-GluCAB-amine-**2** levels. These results were in-line with observations from the image-guided biodistribution for [^{64}Cu]Cu-GluCAB-maleimide-**1**, which is seen to remain in circulation (*i.e.* bound to plasma proteins, such as HSA) as indicated by a ~ 45 to 55-fold higher presence in plasma (10.7 ± 1.8%ID/g) as compared to [^{64}Cu]Cu-TETA (0.25 ± 0.16%ID/g; $p < 0.001$) and [^{64}Cu]Cu-GluCAB-amine-**2** (0.19%ID/g). Consequently, all other organs also show significantly higher activity levels as compared to TETA, in particular the liver uptake of 9.60 ± 1.36%ID/g for GluCAB-maleimide-**1**, which was 25-fold higher than TETA ($p < 0.001$), therefore confirming the hepatobiliary excretion pathway expected for larger protein based compounds. The liver, being a highly perfused organ, also reflects any remaining blood pool ^{64}Cu-activity, which is possible for other organs as well; the %ID/g of the heart (3.15 ± 2.13) was similar to that of the lung (3.21 ± 1.03) and twice as high to that of the spleen (1.33 ± 0.30). Also, notable uptake (with reference to muscle tissue (0.57 ± 0.10%ID/g)), was seen in ovaries and stomach. Interestingly, while the ^{64}Cu-activity in the large intestines was similar between [^{64}Cu]Cu-GluCAB-maleimide-**1** and -amine-**2**, the [^{64}Cu]Cu-GluCAB-maleimide-**1** levels were 4-fold higher than -amine-**2** within the small intestinal tract (Fig. 5).

3. Conclusion

Herein, the first and second phase of a potentially new radioligand designed for tumour-targeting and theranostic capabilities has been completed. The bifunctional chelator GluCAB-maleimide-**1**, has been successfully synthesised, radiolabelled and preliminarily investigated for its *in vivo* albumin-binding capabilities. Towards this end, GluCAB-amine-**2** was successfully radiolabelled with copper-64 and subsequently converted to its radiolabelled GluCAB-maleimide-**1** derivative, which proved to be very stable in serum. *In vivo* studies for [^{64}Cu]Cu-GluCAB-maleimide-**1** clearly estimated a prolonged biological half-life (6–8 h) as compared to the pharmacokinetics of [^{64}Cu]Cu-GluCAB-amine-**2** (lacking the maleimide functionality), and although an elevated liver uptake was noted, an adequate compound excretion was seen within 24 h. These results have translational merit for continuation to phase 3 of the investigation – the evaluation of [^{64}Cu]Cu-GluCAB-maleimide-**1** towards tumour targeting in diseased animal models. However, this study had some limitations which need to be considered such as 1) the high temperature and low pH conditions required for chelator radiolabelling that are not compatible with the sensitive maleimide functional group; and 2) the increased liver uptake - possibly as a result of the complex charge, complex instability *in vivo* or SOD transchelation within the liver. Further studies are under way addressing these limitations, — including *in vitro* studies to confirm targeting of GLUT and the dual-targeting principle of the conjugate – and once accomplished, tumour targeting using [^{64}Cu]Cu-GluCAB-PET/CT imaging can be established.

4. Experimental section

4.1. Synthesis and characterisation of GluCAB-amine-2 and GluCAB-maleimide-1

The full chemical synthesis of all the compounds described in the text can be found in the Supporting Information. Described below is the synthetic method (and characterisation) for compounds (**1**) and (**2**) *via* the protected intermediate compound (**3**) and synthesised components (**4**), (**5**) and (**6**) (Scheme 1). All commercial chemical reagents and solvents were purchased from Sigma Aldrich Chemical Co. Ltd. or Merck (South Africa). Thin layer chromatography was carried out on Silica-gel 60 F_{254} plates (Art. 5554; Merck). Column chromatography was done using Silica-gel 60 from (Merck 7734, 0.040–0.063 mm). Melting points were determined on a Reichert-Jung Thermovar hot-

stage microscope. Infrared spectra were recorded on a Perkin Elmer Spectrum 100 FT-IR Spectrometer using NaCl disks for oils or KBr/compound discs for solids. High-resolution mass spectra were obtained on a Agilent 6530 Accurate-Mass Q-TOF LC/MS with electrospray ionization (ESI) using an Agilent 1290 HPLC fitted with Agilent Eclipse Plus C18 RRHD 1.8 μm 2.1 × 50 mm column. ^{1}H NMR and ^{13}C NMR were recorded on a Varian Mercury 300 MHz (75.5 MHz for ^{13}C), a Varian Unity (400 MHz for ^{13}C) or a Bruker Advance III with Ultra Shield 400 Plus magnet. All spectra were recorded in deuterated chloroform or deuterated water and all chemical shifts were recorded in ppm with reference to the resonance of the residual solvent used as internal standard. For radiolabelling, all solvents used were HPLC grade from Merck and all buffer solutions were prepared using common procedures with Milli-Q grade water (>18 MΩ/cm). The activity of the [^{64}Cu]$CuCl_2$ solution was measured using a Capintec CRC-15R gamma detector (Capintec Inc., Florham Park, NJ, USA). All radiolabelled compounds were analysed by radio-HPLC analysis on Varian Prostar 325 UV–Vis HPLC apparatus (Varian Inc., Walnut Creek, CA, USA) fitted with a radiometric *GABI Star* gamma detector (raytest GmbH, Straubenhardt, Germany) using a Zorbax Stable Bond-C18 column (5 μm; 4.6 × 250 mm) with a gradient elution over 20 min of 95–5% A in B (Solvent A = H_2O (0.1% TFA); Solvent B = MeCN (0.1% TFA)). Purification of the radiolabelled products was done using a pre-conditioned Sep-Pak Light C-18 cartridge (Waters Corporation, Milford, MA, USA). For *in vitro* and *in vivo* studies, samples were centrifuged using a Hettich EBA 20 (A. Hettich GmbH & Co, Tuttlingen, Germany) and automated gamma counting was done using Hidex AMG (LabLogic, Turku, Finland). Serum separation was done using BD Vacutainer® SST™ serum separator tubes (Becton, Dickinson and Company (Franklin Lakes, NJ, USA)).

*4.2. 1-[10-(2,3,4,6-O-tetrabenzoyl-β,D-glucopyranos-1-yl)-1-oxodecyl]-4,11-Bis-(t-butoxycarbonylmethyl)-8-(10-(t-butoxycarbonylamino)-decyl)-1,4,8,11-tetraazacyclotetradecane (**3**)*

Cyclam (**5**) (0.290 g, 0.49 mmol) was reacted with glycosyl bromide (**4**) (0.280 g, 0.34 mmol) and K_2CO_3 (0.204 g, 1.47 mmol) in MeCN (20 mL) to yield 1-[10-(β,D-glucopyranos-1-yl)-1-oxodecyl]-4,11-Bis-(*t*-butoxycarbonylmethyl)-1,4,8,11-tetraazacyclotetradecane (**15**) as a clear oil following purification (0.233 g, 58%)(See supporting information for full reaction and characterisation).

Alkyl bromide (**6**) (0.115 g, 0.34 mmol) was dissolved in MeCN (1 mL) and added to a solution of cyclam (**15**) (0.200 g, 0.17 mmol) in MeCN (10 mL) along with K_2CO_3 (0.071 g, 0.51 mmol). The solution was stirred at 80 °C for 16 h followed by filtration through a small celite pad which was then washed with MeCN (2 mL). The filtrate was concentrated down to leave an oily reside which was purified using column chromatography (CH_2Cl_2:MeOH:NH_4OH, 8.8:1.1:0.1). Some product remained on the column and was flushed out with CH_2Cl_2:MeOH:NH_4OH, 7:2.5:0.5. Compound (**3**) was obtained as a clear oil (0.176 g, 74%); R_f = 0.56 (CH_2Cl_2:MeOH:NH_4OH, 8.8:1.1:0.1); δ_H ($CDCl_3$, 300 MHz): 8.01–7.81 (8H, m, ArH), 7.55–7.25 (12H, m, ArH), 5.89 (1H, t, *J* = 9.6 Hz, H-3Glu), 5.66 (1H, t, *J* = 9.6 Hz, H-4Glu), 5.50 (1H, dd, *J* = 7.8, 9.6 Hz, H-2Glu), 4.83 (1H, d, *J* = 7.8 Hz, H-1Glu), 4.62 (1H, dd, *J* = 3.2, 12.0 Hz, H-6aGlu), 4.50 (2H, dd, *J* = 5.2, 12.0 Hz, H-6bGlu, —NH), 4.14 (1H, m, H-5Glu), 3.89 (1H, dt, *J* = 6.4, 9.6 Hz, OCH_2), 3.53 (1H, dt, *J* = 6.8, 9.6 Hz, OCH_2), 3.38(4H, bs, —NCH_2), 3.19–2.94 (18H, bm, —NCH_2), 2.78–2.68 (4H, bm, —NCH_2), 1.98 (4H, bm, $NCH_2CH_2CH_2$-N), 1.67 (4H, bm, CH_2), 1.50 (2H, m, CH_2), 1.43 (27H, s, CH_3), 1.34–1.01 (26H, m, CH_2-alk); δ_C ($CDCl_3$, 100 MHz): 170.8 (C═O), 170.8 (C═O), [166.2, 165.9, 165.2, 165.0 (C═O)], 156.5 (C═O), [133.4, 133.2, 133.2, 133.1 (ArC)], [129.9 (×2), 129.8 (×2), 129.6 (×2), 129.0 (×2), 128.6, 128.5 (×2), 128.4 (×2), 128.3, 128.1 (×2) (ArC)], 101.3 (C-1Glu), 81.1 (C-^{t}Bu), 81.1 (C-^{t}Bu), 80.5 (C-^{t}Bu), 73.0 (C-3Glu), 72.2 (C-2Glu), 72.0 (C-5Glu), 70.4 (OCH_2), 69.9 (C-4Glu), 63.3 (C-6Glu), 56.1 (CH_2COO),56.1 (CH_2COO), [53.9, 51.8, 51.3 (×2), 51.2 (×2), 50.7 (×2), 49.3 (×2)(C—N)],40.9 (CH_2NHCO), [29.8, 29.7, 29.4 (×2), 29.4 (×2), 29.3 (×4), 29.2 (×2), 28.2 (×2)(CH_3), 28.1(CH_3), 27.2 (x2), 25.8, 25.7, 24.8, 23.7 (CH_2Alk/$NCH_2CH_2CH_2$N)]; ν_{max}/cm^{-1}: 1733 (C═O); HRMS (ESI MALDI-TOF): *m/z* Calculated for $C_{81}H_{119}N_5O_{16}$ (M)$^+$; 1417.8652 found – mass too large, could not be determined.

*4.3. 1-[10-(β,D-glucopyranos-1-yl)-1-oxodecyl]-8-(10-aminodecyl)-4,11-diacetic acid-1,4,8,11-tetraaza-cyclotetradecane (**2**)*

Removal of the benzoyl protecting groups from the glycoside of compound (**3**) was done as follows: Sodium methoxide (25% in MeOH) (0.5 mL) was added to a solution of (**3**) (0.100 g, 0.07 mmol) in anh. MeOH (4 mL) and stirred for 1 h. The reaction was quenched by addition of Dowex H+ to a pH of 5 and stirred for 15 min. Following work-up and purification (see supporting information), 1-[10-(β,D-glucopyranos-1-yl)-1-oxodecyl]-4,11-Bis-(*t*-butoxycarbonylmethyl)-8-(10-(*t*-butoxycarbonylamino)decyl)-1,4,8,11-tetraazacyclotetradecane (**16**) was obtained as a clear oil (0.050 g, 71%).

Cyclam (**16**) (0.050 g, 0.05 mmol) was dissolved in a mixture of CH_2Cl_2:TFA (1:1; 4 mL) and stirred for 16 h at RT. The solvent was evaporated under a stream of air and the oily residue redissolved in 10% NH_4OH in water (1 mL). The product was purified with column chromatography using Alumina N as the stationary phase. The mobile phase for elution of the by-products consisted of a gradient elution with DCM: MeOH:NH_4OH (8:1.7:0.3; 7:2.5:0.5; 6.5:3:0.5) while the product was eluted with MeOH:H_2O (6:4; 4:6). The combined product fractions were concentrated under a stream of air overnight. The residue was redissolved in water (0.5 mL) and desalted by loading onto a Sep-Pak Light C-18 cartridge, washing the cartridge with water (2 mL) and then eluting the product with 50% MeOH in water (2 mL). The solvent was evaporated off under a stream of argon, the residue redissolved in water (1 mL) and freeze-dried (Christ Alpha I-5, Type 1050, Medizinische Apparatebau, Harz, Germany) overnight to yield the title compound, GluCAB-amine-**2** as a lyophilised powder (0.027 g, 69%). δ_H (D2O, 300 MHz): 4.34 (1H, d, *J* = 7.8 Hz, H-1Glu), 3.80 (2H, m, OCH2, H-6aGlu), 3.63–3.56 (4H, m, OCH2, H-6bGlu, —NCH2), 3.49–3.25 (6H, m, H-2/3/4/5Glu, —NCH2), 3.20–2.85(16H, bm, —NCH2), 2.70–2.60 (6H, bm, —NCH2), 1.79 (4H, bm, NCH2CH2CH2N), 1.60–1.50 (8H, bm, CH2),1.29–1.15 (24H, m, CH2-alk)δC(D2O, 100 MHz): 173.8 (C═O), 173.7 (C═O), 102.0 (C-1Glu), 75.8 (C-3Glu), 75.7 (C-2Glu), 73.1 (C-5Glu), 70.6 (OCH2), 69.6 (C-4Glu), 60.7 (C-6Glu), 54.6 (CH2COO), 54.5 (CH2COO), [54.0, 52.5, 51.6, 51.5, 50.6 (×2), 50.0 (×2), 49.6, 49.4 (C—N)], 41.4 (CH2NHCO), [30.8, 30.7, 30.6 (×2), 30.4 (×2), 30.3 (×2), 30.0, 29.2, 28.7, 28.0, 27.8, 27.6, 25.8, 25.7, 22.5, 21.3 (CH2Alk/NCH2CH2CH2N)]; νmax/cm^{-1}: 3345 (OH/NH), 1688 (C═O)HRMS (ESI MALDI-TOF): *m/z* Calculated for C40H79N5O10 (M + H)+; 790.5860;found 790.5887.

*4.4. 4-[10-(4-(2,5-dioxo-2,5-dihydro-1H-pyrrol-1-yl)butanamido)decyl]-11-[10-(β,D-glucopyranos-1-yl)-1-oxodecyl]-1,4,8,11-tetraazacyclotetradecane-1,8-diacetic acid (**1**)*

Maleimido-butyric acid NHS-ester (**18**) (0.005 g, 0.017 mmol) was dissolved in DMF (0.05 mL) and added to a solution of GluCAB-amine-**2** (0.010 g, 0.011 mmol) in 0.01 M PBS (0.40 mL; pH 7.4). The reaction was stirred for 1.5 h at room temperature followed by evaporation of solvent under an air stream. The residue was redissolved in water (0.20 mL) and loaded onto a Sep-Pak Light C-18 cartridge pre-conditioned with EtOH (4.0 mL) and water (2.0 mL). The cartridge was fractionally eluted with water (2 × 2 mL), 10% EtOH/water (2 × 1 mL), 20% EtOH/water (4 × 0.5 mL) and 30% EtOH/water (10 × 0.5 mL). The fractions of 30% EtOH/water were combined and dried under argon to yield the GluCAB-maleimide-**1** (0.006 g, 55%) δ_H (D_2O, 300 MHz): 6.78 (2H, s, CHMal), 4.32 (1H, d, *J* = 7.8 Hz, H-1Glu), 3.86 (2H, m, OCH_2a, H-6aGlu), 3.65–3.56 (4H, m, OCH_2b, H-6bGlu, —NCH_2),3.52 (2H, m, $OCCH_2CH_2CH_2NMal$), 3.49–3.25 (6H, m, H-2/3/4/5Glu, —NCH_2), 3.20–2.85(16H, bm, —NCH_2), 2.70–2.60 (6H, bm,

—NCH_2), 2.17 (2H, m, $OCCH_2CH_2CH_2NMal$), 1.87 (2H, m, $OCCH_2CH_2$-CH_2NMal), 1.79 (4H, bm, $NCH_2CH_2CH_2N$), 1.62–1.50 (8H, bm, CH_2),1.29–1.15 (24H, m, CH_2-alk);δ_C (D_2O, 100 MHz): 174.8 (C═O),173.8 (C═O), 173.7 (C═O), 172.4 (C═OMal), 134.5 (C═C), 102.2 (C-1Glu), 75.9 (C-3Glu), 75.8 (C-2Glu), 73.3 (C-5Glu), 70.8 (OCH_2), 69.9 (C-4Glu), 60.7 (C-6Glu), 54.6 (CH_2COO),54.5 (CH_2COO), [54.1, 52.6, 51.6, 51.6, 50.5 (×2), 50.1 (×2), 49.7, 49.4 (C—N)], 40.4 (CH_2NHCO),38.1 (C-4), 34.2 (C-2), [30.8, 30.7, 30.6 (×2), 30.4 (×2), 30.3 (×2), 30.0, 29.2, 28.7, 28.0, 27.8, 27.6, 25.8, 25.7, 25.6, 22.5, 21.3 ($CH_2Alk/NCH_2CH_2CH_2N$)]; HRMS (ESI MALDI-TOF): *m/z* Calculated for $C_{48}H_{86}N_6O_{13}$ $(M + H)^+$; 955.6286; found 955.6291.

4.5. Isotope preparation

All solutions and buffers were prepared using common procedures using Milli-Q grade water (>18 MΩ/cm). Copper-64 was obtained by irradiation of a CuO (Sigma-Aldrich; 99.9999% purity) powder target (1 mg) for 36 h in the 'in-core' position with a neutron flux of 1×10^{14} n/cm^2/s (8 h cooling period) at the SAFARI-1 research reactor (Necsa, Pelindaba, South Africa). The irradiated copper oxide powder was dissolved in c. HCl (50 μL) and diluted with water (950 μL) to produce a solution of [^{64}Cu]$CuCl_2$. Gamma spectrometry (Canberra Germanium Detector – GC2518 (24% deficiency) (Mirion Technologies, Canberra; Inc. CT, USA)) confirmed presence of the characteristic 511 keV and 1345 keV, emissions of copper-64.

4.6. Radiolabelling

To establish the optimal conditions for radiolabelling of GluCAB-amine-**2** with ^{64}Cu the radiolabelling performance was compared at pH 3.5, 5.0 and 9.0, at temperatures of 45, 70, 80 and 90 °C and reaction times of 10, 20 and 30 min, respectively. Purification of the radiolabelled products was done using a pre-conditioned (4 mL EtOH followed by 2 mL H_2O) Sep-Pak Light C-18 cartridge by loading the reaction solution on the cartridge, washing with water (2 mL) and eluting the labelled product with 50% EtOH/H_2O (1 mL).

4.7. ^{64}Cu-radiolabelling - optimized method

A [^{64}Cu]$CuCl_2$ solution (100 μL; ~10–12 MBq; molar equivalent ligand:metal = 3:1) was added to the GluCAB-amine-**2** in 0.1 M NH_4OAc buffer (100 μL; 10 mg/mL; pH 5.5). The pH of the solution was adjusted with 0.1 M NaOH (60 μL) to pH 3.5, the vial capped and the solution heated for 30 min at 90 °C (Table S1). After the solution had cooled it was purified on a SPE cartridge as indicated. The reaction solution was dried under a stream of argon with heating (60 °C), the residue was re-dissolved in 0.01 M PBS (400 μL) and radio-HPLC analysis performed.

4.8. Post-labelling conversion of [^{64}Cu]Cu-GluCAB-amine-2 to [^{64}Cu]Cu-GluCAB maleimide-**1**

4-maleimidobutyric acid NHS-ester (4.5 μL, 100 μg/μL in DMF, 1.3 eq) was added to the [^{64}Cu]Cu-GluCAB-amine-**2** reaction vial (400 μL, 0.01 M PBS) and stirred for 1 h at room temperature. The reaction solution (400 μL) was purified on a SPE cartridge as described above, dried under argon with slight heating (60 °C) and redissolved in 0.01 M PBS.

4.9. ^{64}Cu-radiolabelling for in vivo studies

A [^{64}Cu]$CuCl_2$ solution (60 μL; 0.72 μmol, 91.5 MBq) was added to a solution of GluCAB-amine-**2** in 0.1 M NH_4OAc buffer (177 μL; 2.24 μmol;10 mg/mL). The pH of the solution was adjusted to pH 3.5 using 2 M NaOH (4 μL), the vial capped and the solution heated for 30 min at 90 °C. Purification was done as mentioned above. The dried [^{64}Cu]Cu-GluCAB-amine-**2** (labelling efficiency of 97%) was redissolved in 0.01 M PBS (900 μL) for *in vivo* application. The production of the maleimide compound included the following steps: After purification, the dried [^{64}Cu]Cu-GluCAB-amine-**2** was redissolved in 0.01 M PBS (400 μL) and 4-maleimidbutyric acid NHS-ester (9 μL, 100 μg/μL in DMF, 1.2 eq) was added to the reaction vial. The reaction was stirred for 1 h at room temperature followed by SPE purification as indicated and drying under a stream of argon with heating (60 °C). The residue was re-dissolved in 0.01 M PBS (900 μL) thereby providing [^{64}Cu]Cu-GluCAB-maleimide-1 (93% conversion, 90% overall yield).

The radiolabelling for the TETA (control compound) was done in a similar manner: [^{64}Cu]$CuCl_2$ solution (60 μL; 0.72 μmol, 91.5 MBq) was added to a solution of TETA in 0.1 M NH_4OAc buffer (150 μL; 1.61 μmol; ligand:metal 2:1). The pH of the solution was adjusted with 2 M NaOH (1 μL) to pH 3.5, the vial capped and the solution heated for 30 min at 90 °C. The product was purified, dried and redissolved in 0.01 M PBS. A labelling efficiency of 95% and radiochemical purity of 99% was obtained.

4.10. Stability and protein binding studies

The *in vitro* stability and serum protein binding studies of [^{64}Cu]Cu-GluCAB-amine-**2** and [^{64}Cu]Cu-GluCAB-maleimide-**1** were completed according to a method previously described [49]. Briefly, the stability was evaluated by adding the desired compound (50 μL, ~10 MBq) to serum (1 mL) and incubating the solution at 37 °C. Samples (100 μL) were drawn at 0, 1, 2, 18 and 24 h after addition of compound and the proteins precipitated by the addition of cold acetonitrile (500 μL). The samples were centrifuged for 10 min at 6000 rpm and the supernatant collected, diluted with MilliQ water and analysed by radio-HPLC (conditions as above). The protein binding was evaluated by addition of the desired compound (25 μL, ~5 MBq) to serum (450 μL) and incubation of the solution at 37 °C. Samples (100 μL) were drawn at 0, 1, 2 and 24 h after administration and the proteins precipitated by the addition of cold acetonitrile (500 μL). The samples were centrifuged for 10 min at 6000 rpm and the supernatant was separated from the protein pellet which was then washed again with acetonitrile (100 μL). The activity of the pellet and supernatant (combined with the wash) was then measured using automated gamma counting and decay-corrected for all samples. The protein binding is expressed as a percentage of the total activity measured.

4.11. Small animal PET/CT imaging

The animal studies were planned and conducted in accordance with the national regulation for the use of laboratory animals for research purposes (SANS 10386). The research was approved by the nationally registered North-West University Animal Care, Health and Safety Research Ethics Committee, (NWU-AnimCare; NWU-00379-16-A5). Female balb/c mice (age: 6–8 weeks; weight: 26 ± 3 g) obtained from the North West University, Preclinical Drug Development Platform (PCDDP) Vivarium (Potchefstroom, South Africa) were housed in individually ventilated cages (Techniplast IVC, Buguggiate, Italy) (*ad libitum* access to water and food, 12 h light/dark cycles and sterile corn-cob bedding). The animals were acclimatised at the Pre-Clinical Imaging Facility (Pelindaba, South Africa) for 1 week prior to commencement of the study. Imaging studies were performed using the small animal PET/CT camera (nanoScanPET/CT, Mediso Medical Imaging Systems, Budapest, Hungary). Mice were randomised and allocated to one of three groups ($n = 5$) as follows: A) [^{64}Cu]Cu-TETA, B) [^{64}Cu]Cu-GluCAB-amine-**2** or C) [^{64}Cu]Cu-GluCAB-maleimide-**1**. The compounds, as indicated per group, were administered intravenously *via* the lateral tail vein ([^{64}Cu]Cu-TETA: 100 μL; 1.2 ± 0.22 MBq; 39 nmol/mouse, [^{64}Cu]Cu-GluCAB-amine-**2**: 150 μL; 5.6 MBq, 31 nmol/mouse and [^{64}Cu]Cu-GluCAB-maleimide-**1**: 100 μL; 1.0 ± 0.09 MBq, 31 nmol/mouse). The animals were anaesthetised using a mix of isoflurane in oxygen (3–4% for induction and 2–2.5% for maintenance). MicroPET/CT image acquisition (CT

scan: time – 5 min, method – semi-circular, zoom – max FOV, binning – 1:4 and image reconstruction: voxel size –medium, filter type - Cosine; PET scan: time – 20 min, coincidence mode – 1-5, prone-head first position) were performed at 1, 2 and 24 h after injection for group A and B and at 1, 2, 4, 8 and 24 h after injection for Group C using the Nucline software (Mediso Ltd., Budapest, Hungary). Qualitative and quantitative analysis was performed on decay-, scatter-, randoms- and attenuation-corrected images using InterView Fusion software (Mediso Ltd., Budapest, Hungary). PET images were normalised (low 0.0; high 10.0) to allow for comparison between different time points and between the three compounds. Image-guided tissue quantification, *i.e.* activity concentration in blood pool (heart) as well as in other organs was done by creating tissue-specific, CT-guided volume-of-interest ('VOI's) areas and each VOI was used to determine the mean standardized uptake value (SUV) (g/mL).

4.12. Biodistribution

Following the imaging studies, the biodistribution of the ^{64}Cu-compounds at 24 h p.i was determined as follows: anaesthetised animals were euthanised by decapitation and blood was immediately collected into a pre-weighed SST™ tubes; serum was yielded by centrifugation (5 min; 6000 rpm). Other tissues and organs were collected into pre-weighed 6 mL plastic vials and the radioactivity of all the samples was measured using automated gamma counting. A standard dilution of the injected activity was performed measuring three volume fractions (100, 200 and 500 μL) to determine the counts/MBq. This value was then used to express the organ activity as a decay-corrected, percentage of the injected dose per gram of tissue (%ID/g).

4.13. Statistics

The protein binding studies were done in triplicate and the data reported as the mean ± standard deviation (SD). The standard uptake values (SUV) determined from microPET/CT analysis and the biodistribution data determined from gamma counting are presented as the mean values and standard deviation (SD). The significance between two mean values of interest was determined by using the two-tailed, equal variance Student's *t*-test. The levels of significance (p) for validating the alternative hypothesis are established at $p < 0.05$, <0.01 or <0.001.

Declaration of competing interest

The authors declare no competing financial interest.

Acknowledgements

The authors acknowledge financial support by the South African Nuclear Energy Corporation (Necsa). Further financial support and infrastructure is acknowledged for pre-clinical studies from the Nuclear Medicine Research Infrastructure, South Africa (NuMeRI) NPC as funded by the Department of Science and Innovation (DSI), South Africa. M.I.P. was jointly supported by the SAMRC with funds received from the National Department of Health, South Africa and the MRC UK with funds from the UK Government's Newton Fund and GSK. The authors would like to thank: Department of Chemistry (University of Cape Town) technical staff for assistance with NMR analysis and the Hunter Research Group for organic synthesis support; Ms M. Buys and Ms B. Marjanovic-Painter (Necsa) for assistance with isotope gamma analysis and HPLC/MS analysis; The staff at the Pre-Clinical Drug Development Platform (PCDDP), NWU, Potchefstroom for assistance with *in vivo* studies and associated veterinary services; Ms. D van Wyk (NuMeRI) and Dr. J. Kleynhans (NuMeRI) for assistance during microPET/CT imaging.

Appendix A. Supplementary data

Details provided include a complete synthesis and characterisation of all compounds indicated in the main manuscript as well as radio-HPLC chromatograms for serum stability analysis of the ^{64}Cu-labelled compounds. Supplementary data to this article can be found online at https://doi.org/10.1016/j.nucmedbio.2021.01.001.

References

[1] Ting G, Chang C-H, Wang H-E, Lee T-W. Nanotargeted radionuclides for cancer nuclear imaging and internal radiotherapy. J Biomed Biotechnol. 2010:953537.
[2] Van Zutphen S, Reedijk J. Targeting platinum anti-tumour drugs: overview of strategies employed to reduce systemic toxicity. Coord Chem Rev. 2005;249:2845–53.
[3] Giancotti FC. Deregulation of cell signaling in cancer. FEBS Lett. 2014;588:2558–70.
[4] Acharya S, Sahoo SK. PLGA nanoparticles containing various anticancer agents and tumour delivery by EPR effect. Adv Drug Deliv Rev. 2011;63:170–83.
[5] a) Maeda H, Bharate GY, Daruwalla J. Polymeric drugs for efficient tumor-targeted drug delivery based on EPR-effect. Eur J Pharm Biopharm. 2009;71:409–19.
b) Fang J, Nakamura H, Maeda H. The EPR effect: unique features of tumor blood vessels for drug delivery, factors involved, and limitations and augmentation of the effect. Adv Drug Deliv Rev. 2009;63:136–51.
[6] a) Matsumura Y, Maeda H. A new concept for macromolecular therapeutics in cancer chemotherapy: mechanism of tumoritropic accumulation of proteins and the antitumor agent smancs. Cancer Res. 1986;46:6387–92.
b) Maeda H, Matsumura Y. Tumoritropic and lymphotropic principles of macromolecular drugs. Crit Rev Ther Drug Carrier Syst. 1986;6:193–210.
c) Maeda H. SMANCS and polymer-conjugated macromolecular drugs: advantages in cancer chemotherapy. Adv Drug Deliv Rev. 1986;46:169–85.
[7] a) Rosenblum D, Joshi N, Tao W, Karp JM, Peer D. Progress and challenges towards targeted delivery of cancer therapeutics. Nat Commun. 2018;9:1410.
b) Kydd J, Jadia R, Velpurisiva P, Gad A, Paliwal S, Rai P. Targeting strategies for the combination treatment of cancer using drug delivery systems. Pharmaceutics. 2018;9:46.
[8] a) Bertrand N, Wu J, Xu X, Kamaly N, Farokhzad OC. Cancer nanotechnology: the impact of passive and active targeting in the era of modern cancer biology. Adv Drug Deliv Rev. 2014;66:2–25.
b) Cho K, Wang X, Nie S, Chen Z, Shin D. Therapeutic nanoparticles for drug delivery in cancer. Clin Cancer Res. 2014;14:1310–13016.
[9] Ramogida CF, Orvig C. Tumour targeting with radiometals for diagnosis and therapy. Chem Commun. 2013;49:4720–39.
[10] Liu S. Bifunctional coupling agents for radiolabelling of biomolecules and target-specific delivery of metallic radionuclides. Adv Drug Deliv Rev. 2008;60:1347–70.
[11] Gutfelin B, Souza SAL, Valentini G. Copper-64: a real theranostic agent. Des Devel Ther. 2018;12:3235–45.
[12] Sun X, Anderson CJ. Production and applications of Copper-64 radiopharmaceuticals. Methods Enzymol. 2004;386:237–61.
[13] Jalilian AR, Osso J. The current status and future of theranostic Copper-64 radiopharmaceuticals. Iran J Nucl Med. 2017;25:1–10.
[14] Paurova M, David T, Cisarova I, Lubal P, Hermann P, Kotek J. Optimization of the selectivity and rate of copper radioisotope complexation: formation and dissociation kinetic studies of 1,4,8-trimethylcyclam-based ligands with different coordinating pendant arms. New J Chem. 2018;42:11908–29.
[15] Wadas TJ, Wong EH, Weisman GR, Anderson CJ. Copper chelation chemistry and its role in copper radiopharmaceuticals. Cur Pharm Design. 2007;13:3–16.
[16] Szymanski P, Fraczek T, Markowicz M, Mikiciuk-Olasik E. Development of copper based drugs, radiopharmaceuticals and medical materials. Biometals. 2012;25:1089–112.
[17] Liu Z, Chen X. Simple bioconjugate chemistry serves great clinical advances: albumin as a versatile platform for diagnosis and precision therapy. X. Chen Chem Soc Rev. 2016;45:1432–56.
[18] Elzoghby AO, Samy WM, Elgindy NA. Albumin-based nanoparticles as potential controlled release drug delivery systems. J Control Release. 2012;157:168–82.
[19] a) Kratz F. Albumin as a drug carrier: design of prodrugs, drug conjugates and nanoparticles. J Control Release. 2008;132:171–83.
b) Kratz F, Ehling G, Kauffmann HM, Unger C. Acute and repeat-dose toxicity studies of the (6-maleimidocaproyl)hydrazone derivative of doxorubicin (DOXO-EMCH), an albumin-binding prodrug of the anticancer agent doxorubicin. Hum Exp Toxicol. 2008;26:19–35.
[20] Miele E, Spinelli GP, Miele E, Tomao F. Albumin-bound formulation of paclitaxel (Abraxane® ABI-007) in the treatment of breast cancer. Int J Nanomedicine. 2009;4:99–105.
[21] Jacobson O, Kiesewetter DO, Chen X. Albumin-binding Evans blue derivatives for diagnostic imaging and production of long-acting therapeutics. Bioconjug Chem. 2016;27:2239–47.
[22] Lau J, Jacobson O, Niu G, Lin K-S, Bénard F, Chen X. Bench to bedside: albumin binders for improved cancer radioligand therapies. Bioconjug Chem. 2019;30:487–502.
[23] Müller C, Farkas R, Borgna F, Schmid RM, Benešová M, Schibli R. Synthesis, radiolabeling, and characterization of plasma protein-binding ligands: potential tools for modulation of the pharmacokinetic properties of (radio)pharmaceuticals. Bioconjug Chem. 2017;28:2372–83.
[24] Upadhyay M, Samal J, Kandpal M, Singh OV, Vivekanakdan P. The Warburg effect: insights from the past decade. Pharmacol Ther. 2013;137:318–30.

[25] Wahl RL. Targeting glucose transporters for tumor imaging: “sweet” idea, “sour” result. J Nucl Med. 1996;37:1038–41.
[26] Smith TA. FDG uptake, tumour characteristics and response to therapy: a review. Nucl Med Comm. 1998;19:97–105.
[27] Morais GR, Falconer RA, Santos I. Carbohydrate-based molecules for molecular imaging in nuclear medicine. Eur J Org Chem. 2013;2013:1401–14.
[28] Feng H, Wang X, Chen J, Cui J, Gao T, Gao Y, et al. Nuclear imaging of glucose metabolism: beyond ^{18}F-FDG. Contrast Media Mol Imaging. 2019;2019:7954854.
[29] Zhang M, Zhang Z, Blessington D, Li H, Busch TM, Madrak V, et al. Pyrophoephorbide 2-deoxyglucosamide: a new photosensitizer targeting glucose transporters. Bioconjug Chem. 2003;14:709–14.
[30] Schibli R, Dumas C, Petrig J, Spadola L, Scapozza L, Garcia-Garayoa E, et al. Synthesis and in vitro characterization of organometallic rhenium and technetium glucose complexes against glut 1 and hexokinase. Bioconjug Chem. 2005;16:105–12.
[31] Weber J, Bollepalli L, Belenguer AM, Di Antonio M, De Mitri N, Joseph J, et al. An activatable cancer-targeted hydrogen peroxide probe for photoacoustic and fluorescence imaging. Cancer Res. August 27 2019. https://doi.org/10.1158/0008-5472.CAN-19-0691.
[32] a) Liang X, Sadler PJ. Cyclam complexes and their applications in medicine. Chem Soc Rev. 2004;33:246–66.
b) Ke CY, Mathias CJ, Green MA. Folate-receptor-targeted radionuclide imaging agents. Adv Drug Deliv Rev. 2004;56:1143–60.
[33] Hunter TM, Paisey SJ, Park H-S, Cleghorn L, Parkin A, Parsons S, et al. Configurations of metallocyclams and relevance to anti-HIV activity. J Inorg Biochem. 2004;98:713–9.
[34] Hoffmann TJ, Smith CJ. True radiotracers: Cu-64 targeting vectors based upon bombesin peptide. Nucl Med Biol. 2009;36:579–85.
[35] Galibert M, Jin Z-H, Furukawa T, Saga T, Fujibayashi Y, Dumy P, et al. RGD-cyclam conjugates: synthesis and potential application for positron emission tomography. Bioorg Med Chem Lett. 2010;20:5422–5.
[36] Murakami T, Sato Y, Shibakami M. Stereoselective glycosylations using benzoylated glucosyl halides with inexpensive promoters. Carbohydr Res. 2008;343:1297–308.
[37] a) Thiem J, Meyer B. Synthesen mit Iod- und Bromtrimethylsilan in der Saccharidchemie. Chem Ber. 1980;113:3075–85.
b) Gervay J, Nguyen TN, Hadd MJ. Mechanistic studies on the stereoselective formation of glycosyl iodides: first characterization of β-D-glycosyl iodides. Carbohydr Res. 1980;300:119–25.
[38] Siwowska K, Haller S, Bortoli F, Benesova M, Groehn V, Bernhardt P, et al. Preclinical comparison of albumin-binding Radiofolates: impact of linker entities on the in vitro and in vivo properties. Mol Pharm. 2017;14:523–32.
[39] a) Pandya DN, Kim JY, Park JC, Lee H, Phapale PB, Kwak W, et al. Revival of TE2A: a better chelator for Cu(II) ions than TETA? Chem Commun. 2010;46:3517–9.
b) Pandya DN, Dale AV, Kim JY, Lee H, Ha YS, An GI, et al. New macrobicyclic chelator for the development of ultrastable ^{64}Cu-radiolabeled bioconjugate. Bioconjug Chem. 2010;23:330–5.
[40] Pandya DN, Bhatt N, Dale AV, Kim JY, Lee H, Ha YS, et al. New bifunctional chelator for ^{64}Cu-immuno-positron emission tomography. Bioconjug Chem. 2013;24:1356–66.
[41] Vimalnath KV, Rajeswari A, Chirayil V, Sharad PL, Jagadeesan KC, Joshi PV, et al. Studies on preparation of ^{64}Cu using (n,γ) route of reactor production using medium flux research reactor in India. J Radioanal Nucl Chem. 2011;290:221–5.
[42] International Atomic Energy Agency. Cyclotron produced radionuclides: emerging positron emitters for medical applications: ^{64}Cu and ^{124}I. IAEA radioisotopes and radiopharmaceuticals reports no. 1. Vienna: IAEA; 2016. p. 3–7.
[43] Xie Q, Zhu H, Wang F, Meng X, Ren Q, Xia C, et al. Establishing reliable Cu-64 production process: from target plating to molecular specific tumour micro-PET imaging. Molecules. 2017;22:641.
[44] Silversides JD, Allan CC, Archibald SJ. Copper(II) cyclam-based complexes for radiopharmaceutical applications: synthesis and structural analysis. Dalton Trans. 2007;9:971–8.
[45] Zarschler K, Kubeil M, Stephan H. Establishment of two complementary in vitro assays for radiocopper complexes achieving reliable and comparable evaluation of in vivo stability. RSC Adv. 2014;4:10157–64.
[46] Jones-Wilson TM, Deal KA, Anderson CJ, McCarthy DW, Kovacs Z, Motekaitis RJ, et al. The in vivo behaviour of copper-64-labeled azamacrocyclic complexes. Nucl Med Biol. 1998;25:523–30.
[47] Bardal SK, Waechter JE, Martin DS. Applied Pharmacology; Chapter 2: Pharmacokinetics. St Louis, MO: Elsevier/Saunders; 2011; 17–34.
[48] Levitt DG, Levitt MD. Human serum albumin homeostasis: a new look at the roles of synthesis, catabolism, renal and gastrointestinal excretion, and the clinical value of serum albumin measurements. Int J Gen Med. 2016;9:229–55.
[49] Beaino W, Anderson CJ. PET imaging of very late antigen-4 in melanoma: comparison of ^{68}Ga- and ^{64}Cu-labeled NODAGA and CB-TE1A1P-LLP2A conjugates. J Nucl Med. 2014;55:1856–63.